THE ROLE OF ATGL-MEDIATED LIPOLYSIS IN DNA DAMAGE AND REPAIR

A DISSERTATION
SUBMITTED TO THE FACULTY OF THE UNIVERSITY
OF MINNESOTA
BY

MAHIMA DEVARAJAN

IN PARTIAL FULFILLMENT OF THE REQUIREMENTS
FOR THE DEGREE OF
DOCTOR OF PHILOSOPHY

Advised by Dr. Douglas Mashek
2025

Acknowledgements

As it is so often the case in situations like this, there is more gratitude to be shared than can be adequately expressed. Scientific advancement is built upon the efforts of those who came before us. With gratitude, I acknowledge their contributions, and I am grateful to have been given an opportunity to make my own contribution to science.

Thanks to all those who have served on my thesis committee the past several years – Dr. Paul Robbins, Dr. Laura Niedernhofer, Dr. Hai Dang Nguyen, Dr. Christina Camell, Dr. Xavier Revelo, Dr. Hai-Bin Ruan. Your feedback and guidance have been invaluable for the development of my project and my development as a scientist.

Thank you to the BMBB program at the University of Minnesota for the support and training opportunities. Thank you to the MSTP program and MSTP leadership, who are simply unparalleled in their leadership and generosity.

Thank you to the Mashek lab members, past and present, whose broad scientific backgrounds helped to curate my multidisciplinary mindset. The pure love of science that exudes from the Mashek lab makes it a joyous environment to work in.

Thank you to my thesis advisor, Dr. Douglas Mashek, for your supportive mentorship over the past several years. You have helped me make scientific connections that have not only served as a useful training experience, but as a reminder that there is never a shortage of ideas to explore. As a result of your mentorship, I am a scientist who believes that the pursuit of science is as much about curiosity and knowledge as it is about service to others.

Finally, thank you to my family and friends, who are (mostly) indulgent of my tediously long scientific musings, are constant sources of inspiration for generosity and service, and are unwavering in their support.

Abstract

An imbalance of DNA damage over repair contributes to the genomic instability that drives aging and countless aging-related diseases. Fasting and caloric restriction are arguably the most well-established interventions that extend lifespan across organisms, a mechanism supported by evidence that fasting can enhance genomic stability. In a fasting state, the upregulation of lipolytic enzymes such as adipose triglyceride lipase (ATGL) leads to the breakdown of lipid droplets (LDs), a process known to impact metabolism and cell signaling. Given the contributory role of LDs and ATGL in the fasting response and the link between fasting and genomic stability, our objective is to elucidate the mechanisms by which LD metabolism regulates genomic stability. We show in multiple cell types that LDs accumulate in response to DNA damage and that ablation of LDs (via inhibition of LD biogenesis) before genotoxic stress increases the persistence of DNA damage and increases senescence. Importantly, we show that overexpression of ATGL (increasing lipolysis) reduces DNA damage and enhances DNA repair in response to both etoposide and ionizing radiation. These findings are recapitulated in mice as genetic lines globally overexpressing ATGL are better able to resolve DNA damage after irradiation. Additional data indicate that pharmacological upregulation of lipolysis can enhance DNA repair, providing both proof of concept for the ATGL studies and an exciting potential intervention for populations undergoing large amounts of DNA damage (e.g., patients undergoing chemotherapy). Finally, our data suggest that ATGL promotes fatty acid oxidation and subsequent production of acetyl-CoA intermediates, which promote acetylation that facilitates DNA repair. Overall, these studies reveal a novel role for LDs and LD proteins in DNA damage and repair, thus unveiling a novel mechanism by which altered metabolism contributes to genomic stability and aging.

Table of Contents

List of Tables

List of Figures

Chapter 1

Chapter 2

Chapter 1:

An Introduction to Lipid Droplets, DNA damage, and DNA repair

DNA damage occurs thousands of times per cell per day. In the ancestral environment, the constant DNA damage faced by early life due to the environment and primitive metabolism demanded the evolution of DNA repair mechanisms for survival and establishment of heredity.[1] As the genome expanded and exogenous/endogenous insults changed, cells evolved multiple mechanisms of DNA repair, and millennia later, human health is still integrally linked with the stability of the genome.

DNA damage and repair

DNA damage can occur from both exogenous (e.g., ionizing radiation, chemotherapeutic drugs) and endogenous sources (e.g., reactive oxygen species, transcription/replication conflicts). DNA lesions include 1) single-base lesions like oxidation, methylation, depurination/deamination, and addition of DNA adducts, 2) multi-base lesions like pyrimidine dimers and DNA cross-links, and 3) single-strand and double-strand breaks (DSBs). DSBs are considered the most dangerous and the most likely to lead to chromosomal rearrangements, mutagenesis, or cell death.

The response to DNA damage can be conceptualized sequentially as recognition of damage, signal amplification, cell cycle arrest, and DNA repair. Upon DNA damage, numerous signaling cascades are initiated to recognize and respond to the damage. One of the earliest events to occur in response to DSBs is the phosphorylation of serine 139 on histone H2AX (commonly denoted γH2Ax) around the break sites.[2,3] γH2Ax initiates the recognition of damage and recruitment of repair proteins and has become widely regarded as a direct marker of DNA damage due to its rapid application to break sites and its specificity to DNA breaks. ATM (ataxia telangiectasia mutated) – a central coordinator of the DNA damage response – is considered the major kinase responsible for H2AX phosphorylation in response to DSBs.[3] After the H2Ax sites in the immediate proximity of the breaks are phosphorylated, more ATM proteins are recruited by DSB- and γH2Ax-sensing complexes, which further phosphorylate more H2Ax sites, leading to signal amplification and additional recruitment of DSB repair proteins. As evidence for the critical role of γH2Ax in DNA repair, mice lacking histone H2AXs show chromosomal

aberrations, higher radiation sensitivity, and failure to recruit repair proteins to their break sites.[4]

In response to DNA damage, cells also make the critical shift from growth and proliferation to cell cycle arrest and DNA repair. After DNA damage, the post-translational modification and accumulation of p53 induces cell cycle arrest though cyclin dependent kinase inhibitor p21, thus increasing the time prior to replication/mitosis for DNA repair to occur.[5] The permanence of this arrest is largely determined by the cell's ability to repair the damage. Cells primarily repair DSBs with nonhomologous end joining (NHEJ) or homologous recombination (HR). NHEJ is an error-prone form of repair, involving direct ligation of broken DNA ends.[6] In contrast, HR is characterized by its ability to utilize a homologous DNA sequence and, therefore, is often considered error-free. During HR, several kilobases around the break site are resected - a process that is antagonized by 53BP1 (a canonical NHEJ protein).[7] Rad51, a commonly used marker for commitment to HR, encapsulates the DNA ends and catalyzes homologous strand invasion, allowing for accurate DNA repair.

Engagement of kinase cascades and post-translational modification of several other signaling/DNA-associated proteins are also important mediators of the DNA damage response (DDR). Several histone modifications, including acetylation, methylation, ubiquitination, and poly-ADP ribosylation are added close to the break site, facilitating the recognition of the break and localization of DNA repair proteins.[8,9] These post-translational modifications of histones and DNA repair proteins have been extensively studied and have been reviewed elsewhere.[9]

Despite multiple coordinated ways to mitigate DNA damage, these are not always sufficient for complete repair, and different scenarios may emerge. If the DNA damage is persistent, it can lead to permanent cell cycle arrest/senescence at the cellular level and premature aging at the physiological level. The profound contribution of DNA damage to aging is evidenced by the fact that mutations in DNA repair proteins lead to

progeroid or early aging syndromes.[10] If the DNA damage is incorrectly repaired, it can lead to acquired mutations and transformation. If the DNA damage is too severe for repair, apoptosis ensues. The balance between DNA damage and the evolved endogenous mechanisms of DNA repair is what dictates genomic integrity, which is inextricably linked to life and death.

Despite decades of accumulated knowledge on DNA damage and DNA repair, DNA damage-associated diseases (cancer, age/senescence-related pathologies, etc.) remain persistent problems. Novel perspectives to understand the cell's response to DNA damage are essential to 1) better understand how cellular endogenous processes contribute to genomic stability or instability, 2) to understand how these processes are altered in the progression of DNA damage-associated diseases, and 3) to provide possible sources of intervention for populations undergoing acute and chronic exogenous DNA damage, such as individuals with DDR protein mutations, patients undergoing chemotherapy treatment, or astronauts pursuing space travel. This thesis explores the novel concept of how two seemingly distinct processes – DNA repair and lipid metabolism – are connected.

Lipid Droplet Biology and Lipolysis

In a seemingly distant part of the cell relative to the nucleus, cytosolic lipid droplets (LDs) serve as a hub of lipid metabolism. Though most prominent in adipose tissue, virtually all cell types can synthesize LDs. LDs store neutral lipids, predominantly triacylglycerols (TAGs) and cholesterol esters (CEs), which are surrounded by a phospholipid monolayer.[11] This monolayer is embedded with LD proteins, which play numerous structural, metabolic, and signaling roles. For instance, the perilipin (PLIN) family of proteins, grouped based on their sequence homology and LD localization, play roles in lipolysis (PLIN1, PLIN2), lipophagy (PLIN2), inflammation (PLIN2), organelle tethering (PLIN5), and nuclear signaling (PLIN5), among others.[12] LDs are dynamic organelles, undergoing expansion, fusion, and catabolism, and interact with most organelles in a regulated manner.

During states of nutrient deprivation, LD catabolism (lipolysis) is essential to meet the energetic demands of the cell. TAG breakdown is first initiated by adipocyte triglyceride lipase (ATGL), the rate-limiting step of lipolysis, in which fatty acids are hydrolyzed from the glycerol backbone, generating diacylglycerol (DAG). The mobilized fatty acid has multiple fates depending on the tissue type and metabolic state, and can be directed towards oxidative metabolism, ketogenesis, signaling, elongation, desaturation, or be re-esterified back into complex lipids such as TAGs and phospholipids. In the subsequent steps of the lipolytic cascade, hormone-sensitive lipase (HSL) cleaves DAG to monoacylglycerol, and monoacylglycerol lipase liberates the remaining fatty acid and glycerol molecule. Mobilized fatty acids can undergo fatty acid oxidation (FAO) upon entry into the mitochondria, generating acetyl-CoA for cellular needs.

As ATGL (also termed desnutrin, gene name is PNPLA2) performs the first and rate-limiting step of lipolysis, its activity is unsurprisingly tightly regulated. ATGL has several binding partners; indeed, proximity labeling studies indicate an ATGL interactome of over 100 proteins.[13] One of the most-studied ATGL-interacting proteins is comparative gene identification-58 (CGI-58, also known as ABHD5), a well-established activator of ATGL-mediated lipolysis. In a basal state, CGI-58 is bound to a PLIN protein, rendering it unable to activate ATGL.[14] In a fasting state, increased β-adrenergic signaling results in the PKA-mediated phosphorylation and activation of HSL, as well as CGI-58. While it does not have lipase activity itself, CGI-58 phosphorylation results in its dissociation from PLIN1/2, freeing it to interact with and activate ATGL. Indicative of the central role CGI58 plays in lipolysis regulation, its interaction with ATGL can increase lipase activity by as high as 20-fold, and its mutation results in ectopic TAG accumulation in non-adipose tissue, much like ATGL loss-of-function mutations.[15,16] The TAG hydrolase activity of ATGL can also be antagonized by interactions with other LD proteins. G0/G1 Switch 2 (G0S2) and hypoxia-inducible lipid droplet-associated (HILPDA) are known ATGL inhibitory proteins that act in different contexts, such as fasting and hypoxia, respectively.[17] To a lesser extent, ATGL activity is also regulated by the perilipins. For

instance, in non-adipose tissue, PLIN2 is more abundant than PLIN1 on the LD, and PLIN2 is thought to act as a physical barrier to restrict ATGL-mediated lipolysis by restricting ATGL access to the LD surface.[18]

ATGL is also under transcriptional control. In maturing pre-adipocytes, peroxisome proliferator-activated receptor gamma (PPARy) induces ATGL expression to promote adipocyte differentiation.[19] Beyond adipogenesis, ATGL expression is also fasting-responsive; binding of forkhead box protein O1 (FoxO1) to the ATGL promoter also stimulates ATGL transcription in low insulin states.[20] Conversely, insulin signaling decreases the expression of ATGL at the transcript level, via suppression of FoxO1.[20] Altogether, ATGL-catalyzed lipolysis is a highly coordinated network that plays a significant role in cellular energetics and function.

Though no crystal structure has been resolved for ATGL at this time, mutational analysis has revealed a C-terminal hydrophobic domain that localizes ATGL to LDs, and like its fellow members of the patatin-like phospholipase domain-containing (PNPLA) family, an N-terminal patatin-like domain.[21,22] The patatin-like domain contains the active site responsible for catalytic lipase activity, and has been shown to bind ATGL modulators like CGI-58 and G0S2.[22,23] Indicative of the importance of ATGL-mediated lipolysis in total body homeostasis, ATGL KO mice show impaired stimulated lipolysis and reduced fasting serum fatty acid levels, accompanied by increased adipose depot size and profound LD accumulation in the heart and liver.[24] In contrast, ATGL overexpression has been shown to reduce LD size, increase lipolysis, and increase TAG turnover.[25,26] Further, adipocyte-specific ATGL overexpression protects against high-fat diet-induced obesity through increased thermogenesis, indicating a central role for ATGL in TAG turnover and body weight regulation.[26] Though predominantly expressed in adipose tissue, ATGL is ubiquitously expressed, notably playing key roles in energy homeostasis in many tissues, including the heart and liver.[17,27] For instance, ATGL is a major TAG lipase regulating lipolysis and the fasting response in the liver.

The absence of liver-specific ATGL is sufficient to drive TAG accumulation and hepatic steatosis on a chow diet, while its overexpression promotes lipolysis and β-oxidation.[28]

While the TAG hydrolase activities of ATGL are well-characterized, other enzymatic functions are beginning to emerge. ATGL has been shown to mobilize retinyl esters in hepatic stellate cells, have phospholipase A2 activity, and have transacylase activity.[29–31] Recently, ATGL has also been shown to mitigate lipopolysaccharide (LPS)-induced inflammation through the cleavage of LPS acylated side chains.[32] The continually emerging roles and regulators of ATGL suggest that the physiological consequences of ATGL overexpression likely extend beyond canonical TAG lipolysis.

LDs and stress

While virtually all cells can store LDs, robust LD accumulation in non-adipose tissues is a commonly regarded indicator of cell stress. LDs have been shown to accumulate in several cell types with stressors like nutrient deprivation, oxidative stress, protein misfolding/endoplasmic reticulum (ER) stress, and acute inflammation.[33,34] At the physiological level, LD accumulation is linked with several disease states such as obesity, cardiovascular disease, nonalcoholic fatty liver disease, neurodegenerative disease, and cancer.[34–36] Beyond mere correlation, LDs have been shown to drive disease and promote cellular senescence.[37–39] Given the strong connections between LDs and cell stressors, it is logical that LD inhibition would mitigate the stress response. Indeed, blocking LD formation or knocking down key LD proteins like PLIN2 has been shown to mitigate such stressors as diet-induced fatty liver disease, sepsis, and acute inflammation.[40–42] However, the converse is also the case; the ability to synthesize LDs has also been shown to mitigate cellular stress. In the context of lipid excess, TAG synthesis has been shown to prevent lipotoxicity by facilitating the storage of lipids into LDs.[43] Further, LD formation has been shown to mitigate ROS-induced damage, ER stress, and lipid peroxidation.[34,44] This paints LDs in a different light, suggesting they are not simply a pathological feature, but a cellular defense. Perhaps the only certainty is that the role of LDs in the management of cellular threats is highly context-dependent,

and thus raises the question of the role LDs play during the existential stress of DNA damage.

Metabolic changes after acute DNA damage

The connection between lipid metabolism and DNA repair has not been extensively studied and is not necessarily intuitive, but it is not without evidence. Upon DNA damage, it stands to reason that the cell must undergo a metabolic shift to adjust to the burden of stress/damage. An existential threat to the cell should demand a halt of non-essential pathways and an upregulation of pathways facilitating recognition and response to that threat. While metabolic shifts in cancer have been thoroughly investigated, these are chronic states resulting from metabolic reprogramming at the transcriptional, translational, and post-translational levels. However, the acute metabolic changes occurring in non-cancer cells following DNA damage remain largely unexplored. Understanding these changes is crucial for understanding how healthy cells mitigate damage and avoid senescent/mutagenic fates.

One metabolic shift that occurs in response to DNA damage is an increased flux towards the pentose phosphate pathway (PPP). The PPP accomplishes two notable functions in the context of DNA repair. First, the ribose-5-phosphate produced from the PPP serves as the sugar backbone of nucleotides and contributes to the nucleotide biogenesis that facilitates DNA repair. Second, during the synthesis of ribose-5-phosphate, NADPH is produced, which contributes to glutathione renewal and mitigation of oxidative stress. Cosentino et al. demonstrate that irradiated human fibroblasts show an increase in G6PD (PPP rate-limiting enzyme) activity, a response which is required for DNA repair and is ablated by ATM inhibition. They further show that the addition of ^{14}C-labeled PPP intermediates is incorporated into RNA after irradiation in an ATM-dependent manner.[45] Additional studies show that inhibition of the PI3-like kinases (including ATM and DNA-PKs) reduces total nucleotide pools through inhibition of the PPP, and subsequently enhances DNA damage.[46] Though mechanistically distinct from DSB repair, defective Nucleotide Excision Repair (NER)

similarly causes reductions in glycolysis and rerouting of glucose towards the PPP.[47] Together, these findings indicate that the metabolic upregulation of the PPP is a key component of DDR programming.

The PPP originates from glycolytic intermediates. However, the effect of acute DNA damage on glycolysis is less clear. Andrabi et al. suggest that the DNA repair regulator PARP-1 activation has an inhibitory effect on glycolysis, though they only manipulated PARP-1 without the addition of an exogenous DNA-damaging agents, so the implication of this study on DNA repair is less clear.[48] Murata et al. used a metric of protein-bound NADH to protein-unbound NADH as a proxy for oxidative phosphorylation (OXPHOS) over glycolysis due to NADH-bound complexes in the electron complex chain. They demonstrate that laser microirradiation-induced DNA damage (as well as H_2O_2 and MMS) increases bound NADH over unbound, suggesting more oxidative phosphorylation and less glycolysis post-DNA damage, an effect that is mitigated with PARP-1 inhibition.[49] They show a decrease in NAD+ and NADH, suggesting increased NAD+ consumption – an expected effect due to increased activity of NAD+ consuming DDR proteins like poly ADP-ribose polymerase (PARP) and sirtuins. Interestingly, inhibitors of oxidative phosphorylation (rotenone and antimycin A), but not glycolysis (2DG), sensitized cells to DNA damage and resulted in a significant decrease in cell survival post-damage, suggesting OXPHOS is required for cell survival post-DNA damage. In support of this, a few studies indicate an acute increase in FAO after multiple types of DNA damage and cell types, and suggest this is critical for cell survival.[50,51] With the stipulation that cancer cells are metabolically divergent from non-transformed cells, acute DNA damage in multiple cancer lines has similarly demonstrated an increase in PPP, a decrease or no change in glycolysis, and an increase in fatty acid oxidation**.** The abundantly studied p53, which is highly activated under states of DNA damage, has also been shown to induce FAO in non-cancer cells.[52]

If glycolysis is reduced acutely after DNA damage, how does the cell provide the necessary substrates for PPP? Jeong et al. used a combination of metabolomics and labeled glutamine tracing to show that MEFs and HepG2 cells decrease glutamine metabolism in response to multiple types of DNA damage (e.g., UV, camptothecin). Specifically, they show a reduction in glutamine uptake and glutamine entry into the TCA cycle while preserving glucose uptake and lactate production.[53] The authors show that this glutamine sparing is regulated by SIRT6 and allows for glutamine to provide nitrogen for nucleotide biosynthesis. Interestingly, they do not show a change in downstream glycolytic intermediates (PEP/pyruvate/lactate), but see an increase in upstream intermediates, such as fructose-6-phosphate that feed into the PPP. In the previously discussed studies, the main measure of glycolysis was ECAR (extracellular acidification rate), which assumes a lactate fate for glycolysis. However, this study suggests that upstream glycolytic flux towards the PPP is elevated post-damage, which potentially would not have a pronounced effect on lactate production. In the context of enhanced FAO, this suggests a model where FAO provides sufficient acetyl-CoA for the TCA cycle while glutamine is redirected towards nucleotide biosynthesis, and upstream glycolysis intermediates can flux towards the PPP to meet the nucleotide biosynthesis demand.

A few studies have performed metabolomics on urine samples collected acutely after irradiation to establish a radiation-induced metabolic profile. In both mouse and human urine samples, acylcarnitines are among the most upregulated metabolites.[54,55] In the context of previous studies showing an increase in OXPHOS post-irradiation, more likely to suggest an increase in acylcarnitine generation, as would be observed with increased lipolysis. As summarized in Figure 1, these studies suggest that acutely after DNA damage, there is a decrease in flux through the glycolytic pathway with diversion of glucose carbons towards PPP, an increase in oxidative phosphorylation and FAO, and a suggestive increase in lipolysis.

Lipid metabolism in DNA damage/senescence

This potential role for lipid metabolism in the DDR extends beyond acute DNA damage, as FAO has become increasingly studied in the context of senescence. Yang et al. have shown that inhibiting fatty acid oxidation (via carnitine palmitoyltransferase I (CPT1) knockdown or etomoxir treatment) increases DNA damage and promotes senescence, consistent with previously described models of acute DNA damage.[56] Acetyl-CoA is a product of increased FAO, and the fate of this acetyl-CoA can have important consequences in the context of DNA damage. Other groups have also shown that FAO plays a protective role in DNA damage by promoting acetylation of DNA repair proteins like PARP-1.[50] Further, chromatin remodeling is an essential component of DNA repair. Modifications of histones, including acetylation, recruit DNA repair proteins to sites of damage.[57] Lipid catabolism is a major source of acetyl-CoA for histone acetylation, with histone acetylation being important to promote HR.[58,59] In contrast, it has also been shown that mitochondrial FAO is elevated in senescent cells and can promote cell cycle arrest and possibly senescence.[60,61] The inhibitory effect of lipolysis on the cell cycle has been previously established, but the presence of enhanced FAO in senescence suggests the possibility that it is a pathogenic adaptation. However, consistent with acute DNA damage studies, these groups show an increase in FAO, acetylcarnitine, increased TCA cycle intermediates with no increases in pyruvate, and decreased glucose utilization in senescent cells. Altogether, the literature demonstrates strong evidence that lipid metabolism plays a role in DNA damage and senescence, though the beneficial or pathological consequences of FAO are likely to depend upon the cell type, basal metabolic state, and the timing post-DNA damage.

In this work, we explore LD dynamics after DNA damage. We show in multiple cell types that LDs accumulate in response to direct DNA damage and that ablation of LDs (via inhibition of LD biogenesis) before administration of DNA-damaging agents increases the persistence of DNA damage and increases senescence. Importantly, we show that overexpression of ATGL (increasing lipolysis) reduces DNA damage and enhances DNA repair in response to both etoposide and ionizing radiation. These findings are

recapitulated in mice as genetic lines globally overexpressing ATGL are better able to resolve DNA damage after irradiation. Additional data indicate that pharmacological upregulation of lipolysis can enhance DNA repair, providing both proof of concept for the ATGL studies and an exciting potential intervention for populations undergoing large amounts of DNA damage (e.g., patients undergoing chemotherapy). Finally, our data suggest that ATGL promotes fatty acid oxidation and subsequent production of acetyl-CoA intermediates, which promote acetylation that facilitates DNA repair. Overall, these studies reveal a novel role for LDs and LD proteins in DNA damage and repair, thus unveiling a novel mechanism by which altered metabolism contributes to genomic stability.

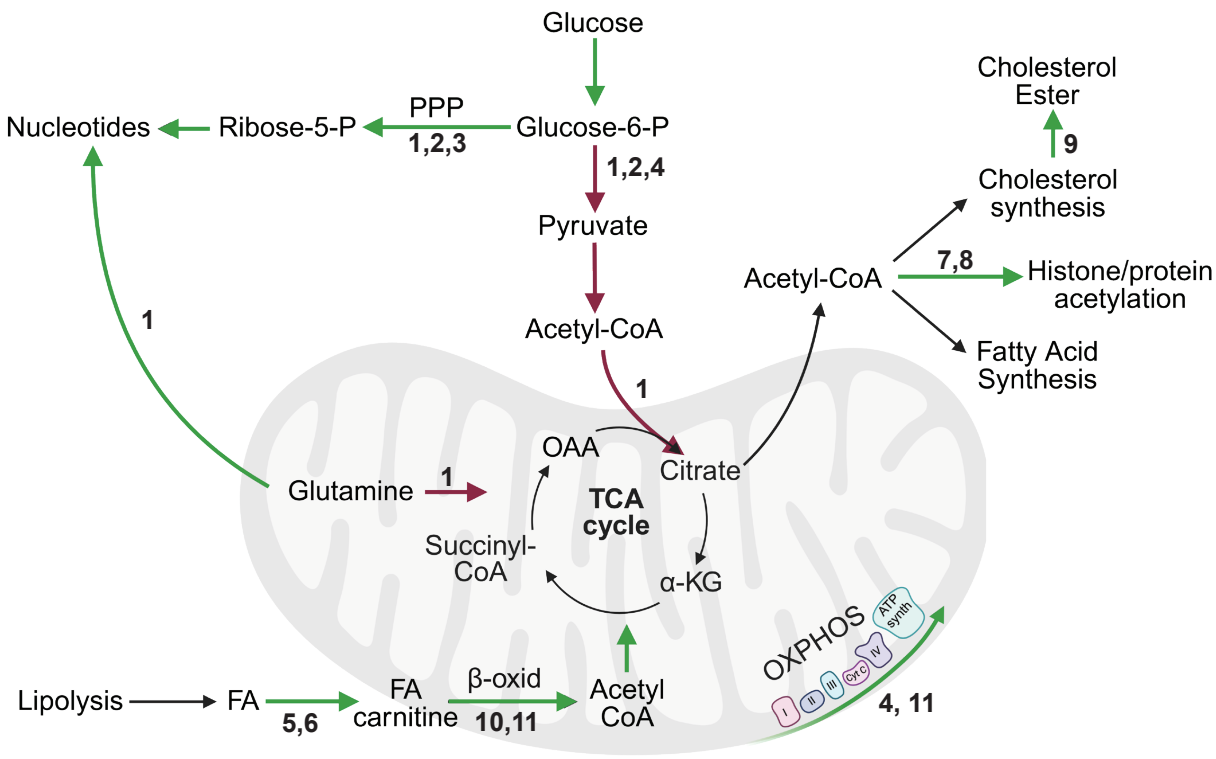

Figure 1. A summarized model of acute metabolic changes after DNA damage in non-cancer cells. Green arrows indicate increased flux after DNA damage. Red arrows indicate decreased flux. 1 – Jeong et al., 2 – Milanese et al., 3 – Cosentino et al., 4 - Murata et al., 5 – Goudarzi et al., 6 – Laiakis et al., 7 – Sivanand et al., 8 – Extensively reviewed, 9 – Overjero et al., 10 – Yang et al., 11 – Brace et al. Abbreviations: FA – fatty acid, OXPHOS – oxidative phosphorylation, TCA – tricarboxylic acid.

Chapter 2:

The role of ATGL-mediated lipolysis on DNA repair

Methods

Mice:

All animal protocols were approved by the University of Minnesota Institutional Animal Care and Use Committee. C57BL/6J mice were maintained on a chow diet (2018 Teklad Global 18% Protein Rodent Diet) with access to water *ad libitum* under a 14/10 light/dark cycle and controlled temperature (23 ± 1°C). Experiments were performed on both male and female mice, unless denoted otherwise.

WT and ATGL floxed mice were of C57BL/6J background. E2A Cre mice (B6.FVB-Tg(EIIa-Cre)C5379Lmgd/J, Jackson Labs) were of B6.FBV background. For the generation of ATGL floxed mice, a construct harboring pAAV-CMV-Beta actin-LOX-STOP-LOX-ATGL FLAG was generated and inserted into the Rosa locus of C57BL/6 mice using a TILD-CRISPR strategy. These mice were crossed with mice expressing E2A Cre (embryonic Cre activation) to generate global ATGL-overexpressing mice carrying a single additional copy of ATGL (AKI). For liver-specific ATGL overexpression, ATGL floxed mice were injected intraperitoneally with AAV8-TBG-iCre (Vector. Biolabs, WB1724), at a dose of $1.4x10^{13}$ GC in 200 µL PBS. Experiments were performed 2 weeks after injection.

Irradiation:

Irradiation (IR) experiments were performed using the RS2000 X-ray irradiator. Mice underwent total body irradiation. Dose-response and time course studies were performed to determine the appropriate dose of IR to induce a γH2Ax response in tissues of interest (7.5 Gy, single exposure, harvest 4 hours post IR). Body weights for all mice were normalized across groups for IR studies to normalize absorbed radiation doses. Sham control mice were placed in the irradiator for the same duration as irradiated mice, without turning on the irradiator.

Cell culture:

All cells, except primary mouse embryonic fibroblasts (MEFs), were maintained in a humidified incubator at 37°C, 5% CO_2. AML12 cells obtained from ATCC were cultured

in DMEM:F12 media supplemented with 10% FBS, 1% ITS (10 mg/mL insulin, 5.5 mg/mL transferrin, 5 ng/mL selenium), 1% Pen/strep, and 50 ng/mL dexamethasone. Primary MEFs were isolated as described.[62] Briefly, breeding pairs were mated and monitored for a vaginal plug. At approximately E13.5, pregnant females were euthanized by CO_2 and embryos were harvested. Embryos were decapitated, and liver and heart were dissected out. The remaining embryonic tissue was manually minced, digested in 0.25% trypsin, and subsequently plated in culture media. Primary MEFs were cultured in 50% DMEM/50% F10 media, supplemented with 10% FBS, 1% nonessential amino acids, 1% pen/strep, and 1% Glutamax. Cells were cultured in a humidified incubator at 37°C in 3% O_2/5% CO_2 for expansion. 24 hours prior to starting experiments, cells were brought to standard culture conditions (5% CO_2, atmospheric oxygen). Primary MEFs were only used up to passage 4 for non-replicative senescence experiments. IMR90 cells were cultured in MEM, 10% FBS, 1% Pen/strep, and 1% Nonessential amino acids. IMR90s were only used up to passage 18 for non-replicative senescence experiments.

For adenoviral transductions, ATGL (Lot: 20160819, mouse ATGL) was obtained from VectorBiolabs, TrackGFP (adGFP) was obtained from UNC Gene Therapy Center, and Null adenovirus was obtained from VectorBiolabs (#1300). AdGFP was used for the control for all non-imaging experiments, and adNull was used for Rad51 imaging experiments and Cytation experiments. Adenoviral transductions were performed in serum-free media. Etoposide treatments were performed 48 hours after the start of transduction.

For measurement of mitochondrial oxidative stress, cells were transfected with Mito RX-RFP plasmid (Addgene 67841) using the Effectene transfection reagent. Cells were transduced with adenoviruses harboring ATGL or a Null control 16 hours later. Twenty-four hours post-transduction, cells were irradiated with 10 Gy, and imaged 3 hours post-IR.

Chemical reagents:

A list of chemical reagents can be found in Table 1.

Table 1. Chemical Reagents

Reagent	Concentration
Etoposide (Millipore 341205)	30μM for acute DNA damage. 10 μM for senescence induction
ATGListatin (Cayman 15284)	50μM
DGAT1 inhibitor – T863 (Sigma SML0539)	20μM
DGAT2 inhibitor - PF-06424439 (Sigma PZ0233)	10μM
SR4995 (Sigma SML2207)	5μM
A485 (p300 inhibitor) (MedChem Express HY-107455)	10μM
CPTH2 (Selleckchem S1242)	50 μM
Avasimibe (MedChem Express HY-13215)	10μM
Nu9056 (AB255734	30μM
WM1119 (SelleckChem S8776)	20μM
6-AN (MedChemExpress HY-W010342)	50 μM
ATMi (KU55933)	10μM
ATRi (AZD6738)	2 μM

Real-time quantitative PCR:

Cells were lysed with Trizol reagent and RNA was extracted using phenol/chloroform separation. RNA was reverse-transcribed to cDNA with the qScript cDNA Synthesis Kit (Quantabio), and then cDNA was amplified using SYBR Green Master Mix for qPCR (Applied Biosystems). β-actin was used as a housekeeping gene. A list of primers can be found in Table 2.

Table 2. RT-qPCR Primers.

Primer	Sequence (F)	Sequence (R)
B-Actin (m)	CAA AAG CCA CCC CCA CTC CTA AGA	GCC CTG GCT GCC TCA ACA CCT C
CDKN1a (m)	TAT CCA GAC ATT CAG AGC CAC A	ACT TTG CTC CTG TGC GGA A
CDKN2a (m)	TGT GCA TGA CGT GCG GG	GCC CAT CAT CAT CAC CTG AAT CG
B-Actin (h)	GGC CGA GGA CTT TGA TTG CA	GGG ACT TCC TGT AAC AAC GCA
CDKN1a (h)	AGT CAG TTC CTT GTG GAG CC	GAC ATG GCG CCT CCT CTG
CDKN2a (h)	TCG GGT AGA GGA GGT GCG	GCC CAT CAT CAT GAC CTG GA
CXCL14 (h)	TAC CGA GGT CAG GAG TG	TTC TTC GTA GAC CCT GCG CT
IFNb (h)	ACG CCG CAT TGA CCA TCT AT	GTC TCA TTC CAG CCA GTG CT
IFNa (h)	GTC AAG CTG CTC TCT GGG CTG	CCA TCA GAC AGG AGG AAG GAG AG
IL1B (h)	GCC AAT CTT CAT TGC TCA AGT GT	AGC CAT CAT TTC ACT GGC GA
IL6 (h)	ACA AGC GCC TTC GGT CCA GTT	CTG AAG AGG TGA GTG GCT GTC TG

NHEJ reporter assay:

The pimEJ5-GFP plasmid from Addgene (44026) was transfected into AML12 cells and selected using puromycin for 2 weeks. Cells were then transduced with adATGL or adNull virus control. The following day, cells were transfected with the I-Sce1 plasmid and mCherry control. 48 hours after SceI transfection, cells were analyzed by flow cytometry. For SR4995 conditions, cells were treated with SR4995 starting the day of Sce-I transfection and maintained in SR4995 for the duration of the experiment. The NHEJ efficiency was calculated as the ratio between GFP+ cells/mCherry+ cells.
We also obtained NHEJ I9a reporter cells in HCA2 fibroblasts from Vera Grobunova and performed the same experiment as above.[63]

Immunofluorescence:

Cells were grown on collagen-coated glass coverslips. Cells were treated with relevant drug pre-treatments, treated with 30 μM etoposide for 3 hours, then recovered in fresh media for 24 hours prior to staining. For immunostaining, samples underwent brief pre-extraction, using 0.1% Triton-X for 2 minutes at 4 degrees. Samples were immediately fixed with 4% PFA for 15 minutes, and permeabilized with 0.5% Triton-X for 15 minutes at room temperature. Samples were blocked with 5% BSA for 1 hr, followed by overnight antibody incubation. Antibody concentrations were: Rad51 (ab133534), 1:200; γH2Ax (Cell Signaling 9719S), 1:250. Images were taken on a Leica DMi8 epifluorescence scope. BODIPY 493/503 staining was performed for 20 minutes at 2 μM.

Senescence staining: The Senescence-Associated β-Gal Staining Kit was purchased from Millipore (CS0030) and was performed according to the manufacturer's instructions. Cells were treated with 20 μM etoposide for two days and allowed to recover for 5 days. Cells were fixed using the kit's fixative and stained with Xgal solution for 12 hours.

Isotope labeling experiments: Pulse-chase experiments were performed as described.[64] Briefly, AML12 cells were treated with an adenovirus harboring ATGL or GFP. 48 hours after transduction, cells were pulsed with 200 μM oleate and [1-^{14}C]oleate (0.1 uCi/μL) bound to FA-free BSA in a 3:1 molar ratio for 4 hours. Etoposide was added to start the chase period. Cells were harvested 4 hours and 16 hours after etoposide treatment. Lipids were extracted and separated by thin layer chromatography to separate major lipid species (phospholipids, cholesterol, DAG, free fatty acids, TAG, CE). Total radiolabeled lipids were quantified by scintillation counter (LS6000, Beckman).

Western blotting:

Cells were harvested in lysis buffer (150 mM NaCl, 10 mM Tris HCl, and 1% Triton X). Prior to protein determination, lysates were sonicated 2x at 15% amplitude. Protein lysates were subjected to SDS-polyacrylamide gel electrophoresis and transferred to PVDF membrane prior to immunoblotting. Membranes were incubated with primary antibody overnight at 4°C. Antibodies used were: γH2Ax (Bethyl A300-081A) at 1:2000; ATGL (Cell Signaling 2138S) at 1:1000, β-actin (A2228) at 1:5000, 53BP1 (Ab36823) at 1:1000, pan-acetylated lysine (Cell Signaling 9681S) at 1:1000.

Comet assay:

Neutral comet assays were performed on AML12 cells using R&D Biosystems 4250-050-K kit. Cells were treated with an adATGL adenovirus or an adGFP control. 48 hours after transduction, cells were treated with etoposide. After 24 hours in etoposide, the comet assay was performed following the manufacturer's instructions. Images were analyzed using OpenComet software.

Cell Viability:

Cells were seeded in a 96-well plate. After drug treatments, wells were incubated in etoposide for 36 hours. Cell Viability was determined using the Alamar Blue assay (Invitrogen DAL1025). Fluorescence intensity at 580 nM was measured 2-4 hours after the Alamar Blue reagent was added to cells.

Lipidomics:

Livers were harvested from irradiated WT or AKI mice. To obtain LD fractions, livers were dissociated with a Dounce homogenizer. Cells were sheared with a 28-gauge needle 10-20 times, then centrifuged at 7500xg for 5 minutes. The fat cake was separated, and hypotonic lysis medium (20 mM Tris-Cl, pH 7.4, 1 mM EDTA, protease inhibitor, phosphatase inhibitor) and 60% sucrose were added. 20% and 5% sucrose were overlaid. Samples were spun at 4°C at 28,000xg for 3 hours.

Lipidomics was performed by Danni Li at the University of Minnesota by direct infusion mass spectrometry. Samples were measured in triplicate. The ratio of each lipid (peak

area for each lipid divided by its corresponding deuterated internal standard) was used to represent relative quantities. To be above noise levels, we only considered lipids whose ratios were three times higher than the corresponding ratio in the blanks. Analysis was performed using LipidSuite.

Cellular ROS:

Cellular ROS was measured using the DCFDA / H2DCFDA - Cellular ROS Assay Kit (ab113851). After etoposide treatment, cells were stained with CDFDA for 45 minutes in phenol red-free media. Fluorescence intensity was measured at 535 nm using a 96-well microplate reader.

8-oxo-DG measurement:

DNA was extracted from 10 mg of liver tissue, and 8-oxo-dG measurement was performed per manufacturer's instructions (R&D Biosystems, Catalog # 4380-096-K)

Chromatin Fractionation:

A method was largely adapted from a previously published protocol.[65] Briefly, cells were lysed with 5 volumes of E1 buffer (50 mM Hepes-KOH pH 7.5, 140 mM NaCl, 1 mM EDTA pH 8.0, 10% glycerol, 0.5% NP-40, 0.25% Triton X-100, 1 mM DTT) complemented with 1x protease inhibitor, phosphatase inhibitor, and deacetylase inhibitor cocktail. The supernatant was collected as the cytoplasm fraction, and the pellet was washed with E1 buffer twice with centrifugation in between. The pellet was resuspended by gentle pipetting in 2 volumes of ice-cold E2 buffer (10 mM Tris-HCl pH 8.0, 200 mM NaCl,1 mM EDTA pH 8.0, 0.5 mM EGTA pH 8.0) complemented with 1x protease and phosphatase inhibitor, and deacetylase inhibitor and spun at 1100xg at 4°C for 2 min. The pellet was resuspended in the same volume of E2, an aliquot was taken as the nuclear fraction, and centrifuged as before. The pellet was washed in E2 buffer twice more with centrifugation at 1100xg for 2 minutes in between. The supernatant was discarded, and the pellet was resuspended in ice-cold E3 buffer (500 mM Tris-HCl, 500 mM NaCl) complemented with 1x protease inhibitor cocktail,

phosphatase inhibitor, and deacetylase inhibitor. The solution (chromatin fraction) was sonicated at 20% amplitude for 10 seconds 3x. Fractions were centrifuged at 16,000xg at 4°C for 10 min, and protein concentration was determined using the BCA protein assay kit.

Flow Cytometry:

Wild type and ATGL-overexpressing MEFs or AML12s were cultured in 6-well plates with DMSO or Etoposide (30 μM) for up to 48 hours. Following, cells were lifted, centrifuged, and fixed in 200 μL of PBS and 100 μL of 4% PFA for 15 minutes at room temperature. Cells were then washed with FACS buffer (PBS, 1% BSA, 0.5 mM EDTA) and stained with BODIPY 493/503 (2 μM) for 30 minutes at room temperature. Finally, they were washed, centrifuged, and resuspended in FACS buffer for flow cytometry data acquisition. Flow cytometry data were acquired with a FACSymphony A3 flow cytometer (BD Biosciences) and analyzed with FlowJo software (BD Biosciences). Relative lipid accumulation was calculated as the mean fluorescence intensity (MFI) of BODIPY in single cells.

Results:

LD ablation prior to genotoxic stress increases DNA damage

Given the pro-inflammatory roles for LDs and the benefits of their ablation, we tested whether ablating LDs prior to genotoxic stress would affect the cell's response to DNA damage, hypothesizing this would reduce DNA damage burden and senescence markers. We chose to test this by blocking TAG formation via inhibition of the DGAT enzymes, which are responsible for the formation of TAG from DAG (Fig 1A). As knockout of DGAT1 or DGAT2 alone still allows for LD formation, we chose to inhibit both DGAT1 and DGAT2 together to ensure no LD biogenesis. DGAT1/2 inhibition for 24 hours was sufficient to starkly reduce LDs in both low-passage and high-passage (LD-laden) IMR90 fibroblasts (Fig 1B). We then pretreated IMR90s with DGAT1/2 inhibitors for 24 hours, followed by 6 hours of etoposide, a topoisomerase II inhibitor and a DSB inducer. Surprisingly, cells pre-treated with DGAT1 and DGAT2 inhibitors

showed more DNA damage (γH2Ax) than cells treated with etoposide alone (Fig 1C). Further, cells pre-treated with DGAT inhibitors showed increased senescence markers as measured by SA-β-galactosidase staining and expression of cell cycle arrest genes, CDKN1a and CDKN2a (Fig 1D). Contrary to the increase in β-gal staining, DGAT inhibition either reduced or did not alter transcription of senescence-associated secretory phenotype (SASP) components (Fig 1E), suggesting a model in which these cells are damaged and cell cycle arrested, but do not express a profound SASP due to LD ablation. Contrary to expectations, these data show that DGAT inhibition worsens etoposide-induced DNA damage, suggesting that the presence of LDs plays a protective role in the response to DNA damage.

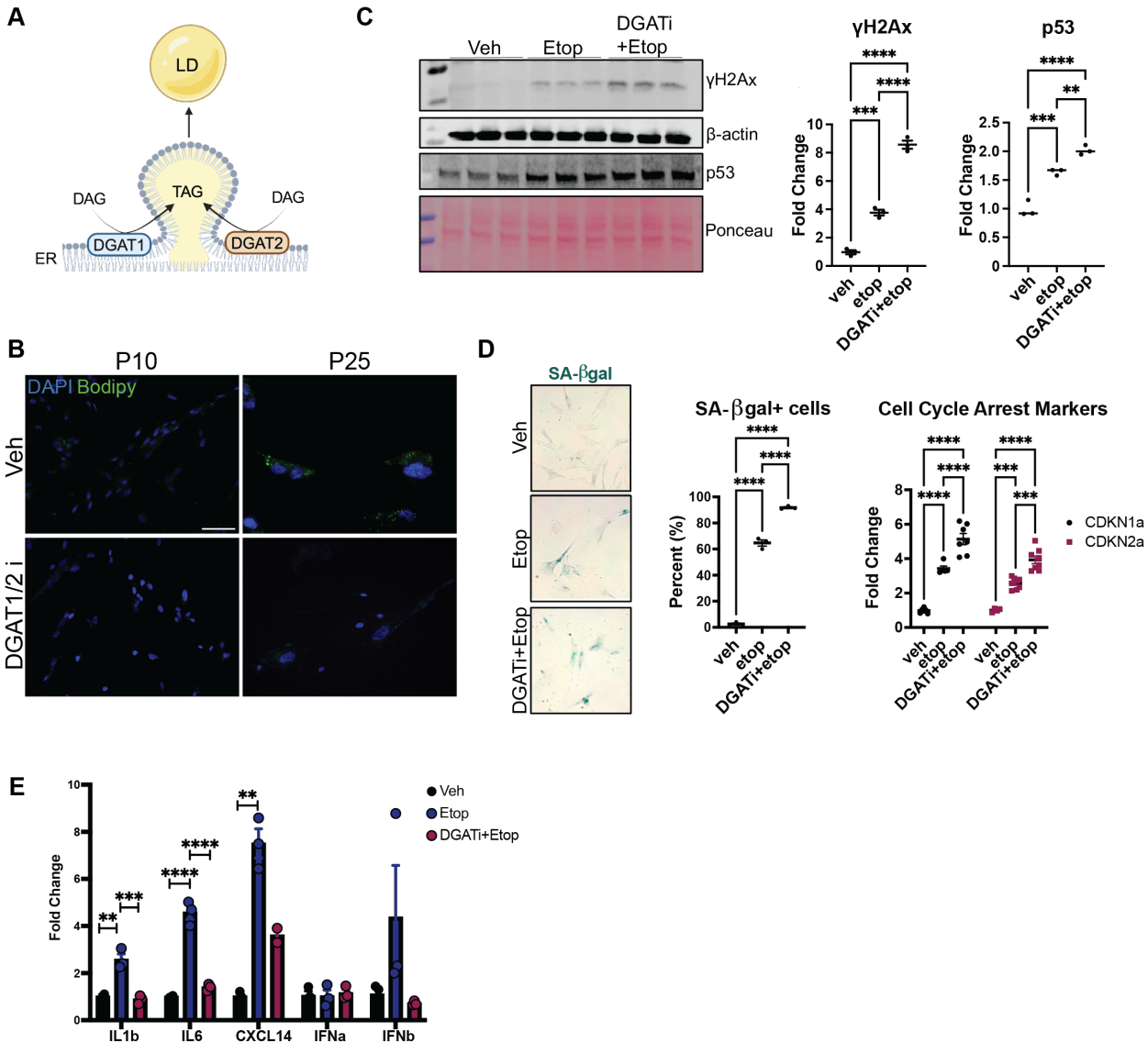
A
LD
DAG
TAG
DAG
ER
DGAT1
DGAT2
B
P10
P25
DAPI Bodipy
Veh
DGAT1/2 i
C
Veh
Etop
DGATi +Etop
γH2Ax
β-actin
p53
Ponceau
γH2Ax
p53
Fold Change
veh
etop
DGATi+etop
D
SA-βgal
Veh
Etop
DGATi+Etop
SA-βgal+ cells
Percent (%)
Cell Cycle Arrest Markers
Fold Change
CDKN1a
CDKN2a
E
Veh
Etop
DGATi+Etop
Fold Change
IL1b
IL6
CXCL14
IFNa
IFNb

Figure 1. DGAT1/2 inhibition prior to genotoxic stress increases DNA damage and senescence. A) DGAT mechanism of action. **B)** IMR90s were treated with DGAT1 inhibitor T863 (20 μM) and DGAT2 inhibitor PF-06424439 (10 μM) for 24 hours. Cells that are low passage (P10) or high passage and LD-laden (P25) both lose LDs after 24 hours of DGAT1/2 pretreatment. Cells were stained with BODIPY 493/503. Scale bar = 100 microns. **C)** IMR90s were treated with DGAT1/2 inhibitor for 24 hours, followed by 6 hours of etoposide treatment and western blot for γH2Ax and p53. Statistics: one-way ANOVA with Tukey's post hoc test. Error bars on graphs indicate mean +/- SEM. ** = $p<0.05$, *** = $p<0.0005$, **** = $p<0.0001$ **D)** Senescence readout of IMR90s pre-treated with DGAT inhibitors. IMR90s were treated with 10 μM etoposide for 48 hours, followed by 5 days of recovery. Beta-galactosidase staining (left) and RT-qPCR for cell cycle arrest markers (right). **E)** RT-qPCR of SASP genes. IMR90s were pretreated with DGAT1/2 inhibitor for 24 hours, followed by 48 hours of 25 μM etoposide treatment, and 6 days of recovery. Cells were kept in the DGAT1/2 inhibitor for the duration of the senescence induction. Statistics: one-way ANOVA (comparisons within genes). Error bars on graphs indicate mean +/- SEM. ** = $p<0.05$, *** = $p\leq0.0005$, **** = $p<0.0001$

ATGL overexpression reduces DNA damage *in vivo* and *in vitro*

The literature suggests that cells upregulate fatty acid oxidation and oxidative phosphorylation after DNA damage, while deprioritizing glycolysis.[51,53] One possible explanation for our DGAT inhibitor data is that by preventing LDs from accumulating, the cells are deprived of substrate for lipolysis/FAO, potentially interfering with the DNA damage response. To test if enhanced lipolysis confers a benefit on DNA damage, we overexpressed ATGL, thus promoting lipolysis in cells before DNA damage. Remarkably, cells overexpressing ATGL showed reduced DNA damage at multiple time points of etoposide treatment (Fig 2A,B). Etoposide preferentially causes DNA damage during the S/G2 phases of the cell cycle, resulting in G2/M stalling. Though we observe minimal effects of ATGL overexpression on the cell cycle (Fig 3A), we sought to test if the ATGL overexpression still conveyed benefit with an insult that causes DNA damage agnostic of the cell cycle. Thus, we used gamma radiation, which causes robust DSBs independent of the cell cycle. As expected, 10 Gy of gamma irradiation caused a robust increase in DNA damage in both control and ATGL overexpression cells immediately after irradiation (Fig 2C,D). However, after 24 hours of recovery, the DNA damage in ATGL-overexpressing cells returned to unirradiated levels while those expressing GFP showed limited recovery (Fig 2D). Given that the baseline damage acquired was the same, this data suggests that ATGL overexpression enhances γH2Ax resolution, and possibly DNA repair.

To confirm that this effect on DNA damage was not an off-target effect of ATGL overexpression, we pretreated AML12 cells with DGAT inhibitors and subsequently overexpressed ATGL (thus overexpressing ATGL in cells without LDs). Importantly, overexpression of ATGL reduced γH2AX, but this effect was abrogated with DGATi pretreatment (Fig 2F). Further, we performed neutral comet assays to directly assess DNA breaks. In agreement with γH2Ax data, ATGL overexpression reduced DNA damage (tail moment), an effect abrogated by pretreatment with DGAT inhibitors (Fig 2G). Together, these data show that the presence of LDs is required for the benefit of

ATGL overexpression, suggesting that it is enhanced LD breakdown (lipolysis) that conveys the benefit of ATGL-mediated DNA repair.

Next, to test this effect *in vivo*, we generated mice globally overexpressing ATGL. A construct harboring pAAV-CMV-Beta actin-LOX-STOP-LOX-ATGL FLAG was generated and inserted in the Rosa locus of C57BL/6 mice using a TILD-CRISPR strategy. These mice were crossed with mice expressing E2A Cre (embryonic Cre activation) to generate global ATGL-overexpressing mice carrying a single additional copy of ATGL (AKI) (Fig 3D,E). We first performed the dose-response/time courses of gamma irradiation in WT mice and determined that doses of 5-10 Gy of irradiation were sufficient to induce DNA damage in multiple tissues and that the γH2Ax signal was substantially reduced by 6 hours post-irradiation (Fig 3B,C). Based on this, we chose to irradiate mice with 7.5 Gy and allow for 4 hours of recovery to assess differences in DNA damage. Consistent with cell culture data, AKI mice showed significantly less γH2Ax 4 hours post-irradiation in the liver, lung, kidney, and heart relative to Cre-negative sham controls.

Though ATGL overexpressing mice have been shown to have normal levels of serum fatty acids, it is a possibility that mobilized fatty acids from the adipose tissue are driving the protective effects in other tissues via the uptake of adipose-derived fatty acids.[26] To test if the observed reduction in γH2Ax effect is due to a cell-nonautonomous effect, we injected male heterozygous ATGL floxed mice with an AAV8-TBG-iCre to generate liver-specific ATGL overexpressing mice. Liver-specific ATGL overexpression was sufficient to induce a similar reduction in γH2Ax after irradiation, suggesting a cell-autonomous effect (Fig 3F), consistent with results from cell culture.

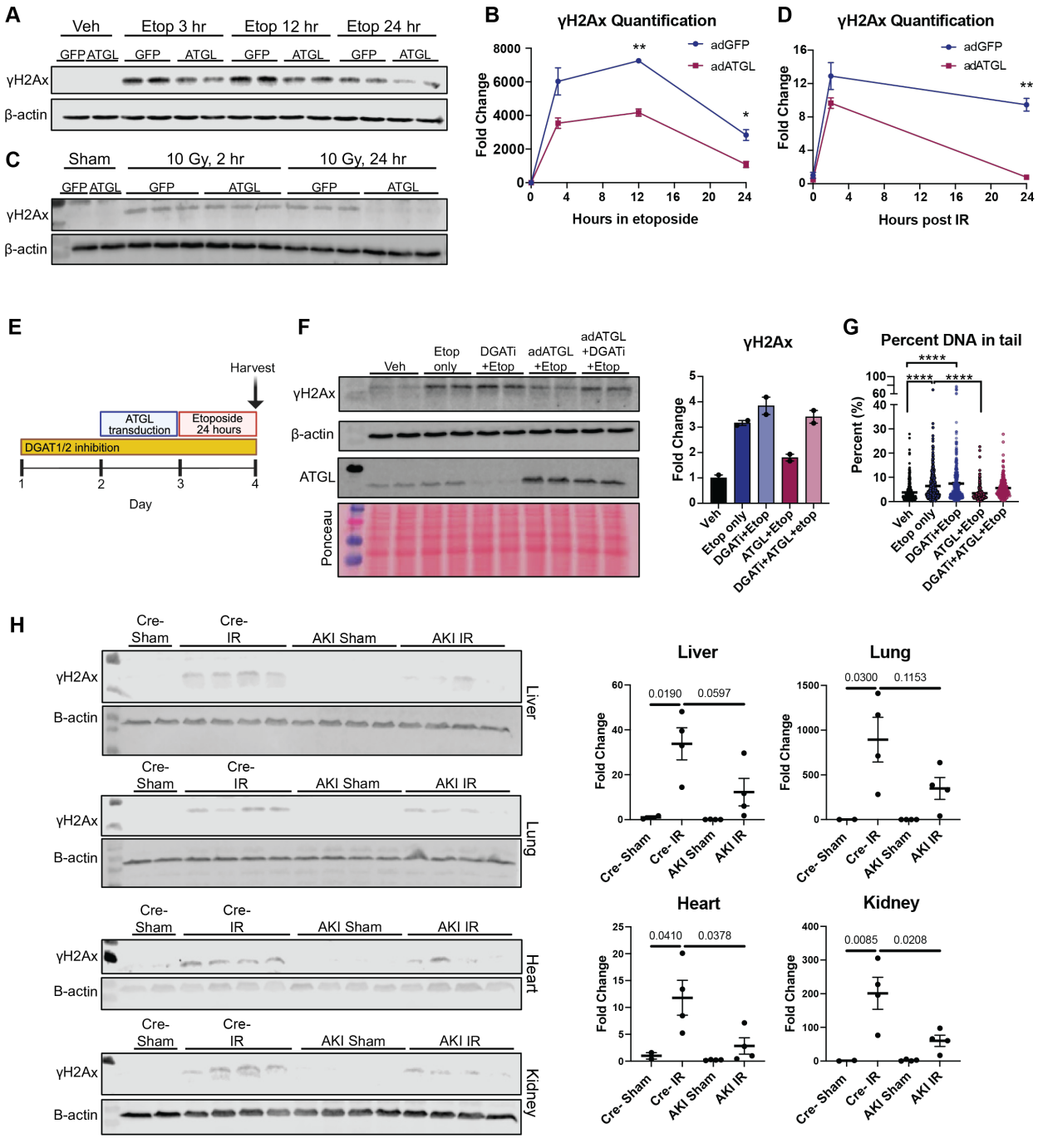
A
Veh
Etop 3 hr
Etop 12 hr
Etop 24 hr
GFP ATGL GFP ATGL GFP ATGL GFP ATGL
γH2Ax
β-actin
C
Sham
10 Gy, 2 hr
10 Gy, 24 hr
GFP ATGL GFP ATGL GFP ATGL
γH2Ax
β-actin
B
γH2Ax Quantification
adGFP
adATGL
Fold Change
Hours in etoposide
D
γH2Ax Quantification
adGFP
adATGL
Fold Change
Hours post IR
E
Harvest
ATGL transduction
Etoposide 24 hours
DGAT1/2 inhibition
Day
F
Veh
Etop only
DGATi +Etop
adATGL +Etop
adATGL +DGATi +Etop
γH2Ax
β-actin
ATGL
Ponceau
γH2Ax
Fold Change
Veh
Etop only
DGATi+Etop
ATGL+Etop
DGATi+ATGL+etop
G
Percent DNA in tail
Percent (%)
Veh
Etop only
DGATi+Etop
ATGL+Etop
DGATi+ATGL+Etop
H
Cre- Sham
Cre- IR
AKI Sham
AKI IR
γH2Ax
B-actin
Liver
Lung
Heart
Kidney
Liver
Lung
Heart
Kidney
Fold Change
0.0190
0.0597
0.0300
0.1153
0.0410
0.0378
0.0085
0.0208
Cre- Sham
Cre- IR
AKI Sham
AKI IR

Figure 2. ATGL overexpression reduces DNA damage. A) AML12 cells transduced with ATGL or GFP control adenoviruses were treated with 30 μM etoposide for the indicated times and assayed for γH2Ax. **B)** Quantification of A. * = $p<0.05$, ** = $p<0.005$. **C)** AML12 cells transduced with ATGL or GFP control adenoviruses were irradiated (10 Gy) and harvested at the indicated times post-IR. **D)** Quantification of C. ** = $p<0.005$. **E)** Schematic of ATGL/LD ablation experiment. **F)** Western blotting for γH2Ax, β-actin, and ATGL. Quantification of γH2Ax was performed relative to β-actin. **G)** AML12 cells were treated as shown in E. The Comet assay was performed on cells after 24 hours of etoposide. Comets were quantified with OpenComet software. A minimum of 180 comets were quantified per condition. Statistics: one-way ANOVA with Tukey's post hoc test. **** = $p<0.0001$. **H)** γH2Ax results and quantification from tissues harvested from E2A Cre-ATGL (AKI) mice irradiated with 7.5 Gy + 4 hr recovery. Mice were of mixed sexes, n=4 mice. P-values from one-way ANOVA are displayed.

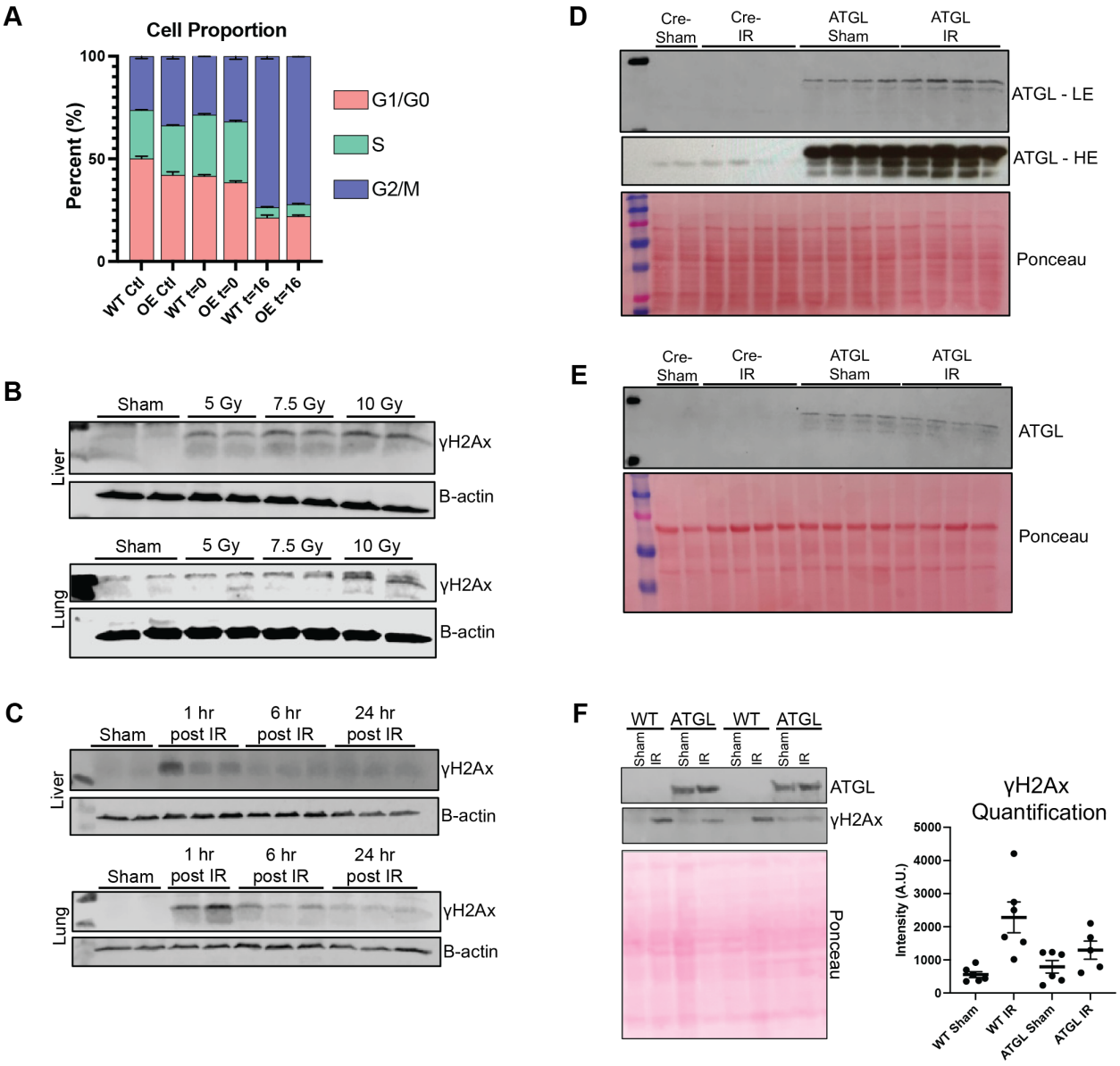
A
Cell Proportion
100
50
0
Percent (%)
G1/G0
S
G2/M
WT Ctl
OE Ctl
WT t=0
OE t=0
WT t=16
OE t=16
B
Sham
5 Gy
7.5 Gy
10 Gy
Liver
γH2Ax
B-actin
Lung
C
1 hr post IR
6 hr post IR
24 hr post IR
D
Cre- Sham
Cre- IR
ATGL Sham
ATGL IR
ATGL - LE
ATGL - HE
Ponceau
E
ATGL
F
WT
ATGL
Sham
IR
γH2Ax Quantification
Intensity (A.U.)
5000
4000
3000
2000
1000
0
WT Sham
WT IR
ATGL Sham
ATGL IR

Figure 3. Additional data related to Figure 2. A) Propidium iodide staining of control and ATGL overexpressing cells with etoposide treatment. “WT ctl”= null virus, no etoposide. “OE Ctl” = ATGL overexpression, no etoposide. “t=0” =cells harvested acutely after 3 hr in etoposide. “t=16” = cells harvested 16 hours after etoposide removal. **B)** γH2Ax dose response in WT mice at indicated IR doses. **C)** γH2Ax time course, harvested at indicated times post-IR. **D,E)** Validation of ATGL overexpression in E2A Cre-AKI liver (D) and lung (E). **F)** γH2Ax and ATGL expression from the livers of ATGL floxed mice that were treated with TBG-iCre for liver-specific ATGL overexpression. Mice were irradiated with 7.5 Gy total body irradiation and harvested 4 hours later.

ATGL/lipolysis promotes DNA repair

Given that ATGL promotes γH2Ax resolution, we sought to further investigate ATGL’s role in DNA repair by measuring markers of HR and NHEJ. To assess HR, we measured Rad51 foci 24 hours after etoposide removal, which indicates Rad51 localization to the chromatin and progression of homology-directed repair. ATGL-overexpressing cells had increased total Rad51 foci, with a trending decrease in total γH2Ax foci (Fig 4A-C). Further, ATGL increased the overlap of Rad51 and γH2Ax signal, indicating that the sites of damage have recruited more Rad51 to facilitate repair (Fig 4D). To interrogate if ATGL promotes NHEJ, we performed chromatin enrichments to assess how ATGL changes the localization of the NHEJ-promoting protein 53BP1. ATGL appears to promote 53BP1 recruitment to the chromatin acutely after DNA damage (3 hours post-etoposide). Interestingly, ATGL increases localization of 53BP1 to the chromatin even without DNA damage, suggesting a priming effect, in which lipolysis activation prior to damage gives the cell a greater capacity to repair the DNA once damage occurs (Fig 4E). To functionally test if NHEJ-mediated repair was occurring, we employed the widely used NHEJ reporter assay. This utilizes a fluorescent construct (pimEJ5GFP) that contains a Sce-I cut site. A plasmid encoding the Sce-I endonuclease is transfected into cells and cuts at its designated site, resulting in GFP fluorescence upon successful in-frame NHEJ repair. We coupled these

experiments with the use of SR4995, a known lipolysis activator. SR4995 binds the ATGL co-activator CGI-58, promoting its dissociation from perilipin proteins and allowing its binding and subsequent activation of ATGL.[66] When measured by flow cytometry 48 hours after the introduction of Sce-1, we observe an approximate doubling of GFP-positive cells overexpressing ATGL (Fig 4F). Notably, we observed a stark induction of GFP-positive cells when cells were pretreated with SR4995. We were able to demonstrate this induction in NHEJ in both liver cells and human fibroblasts, suggesting this effect is conserved across cell types (Fig 4G).

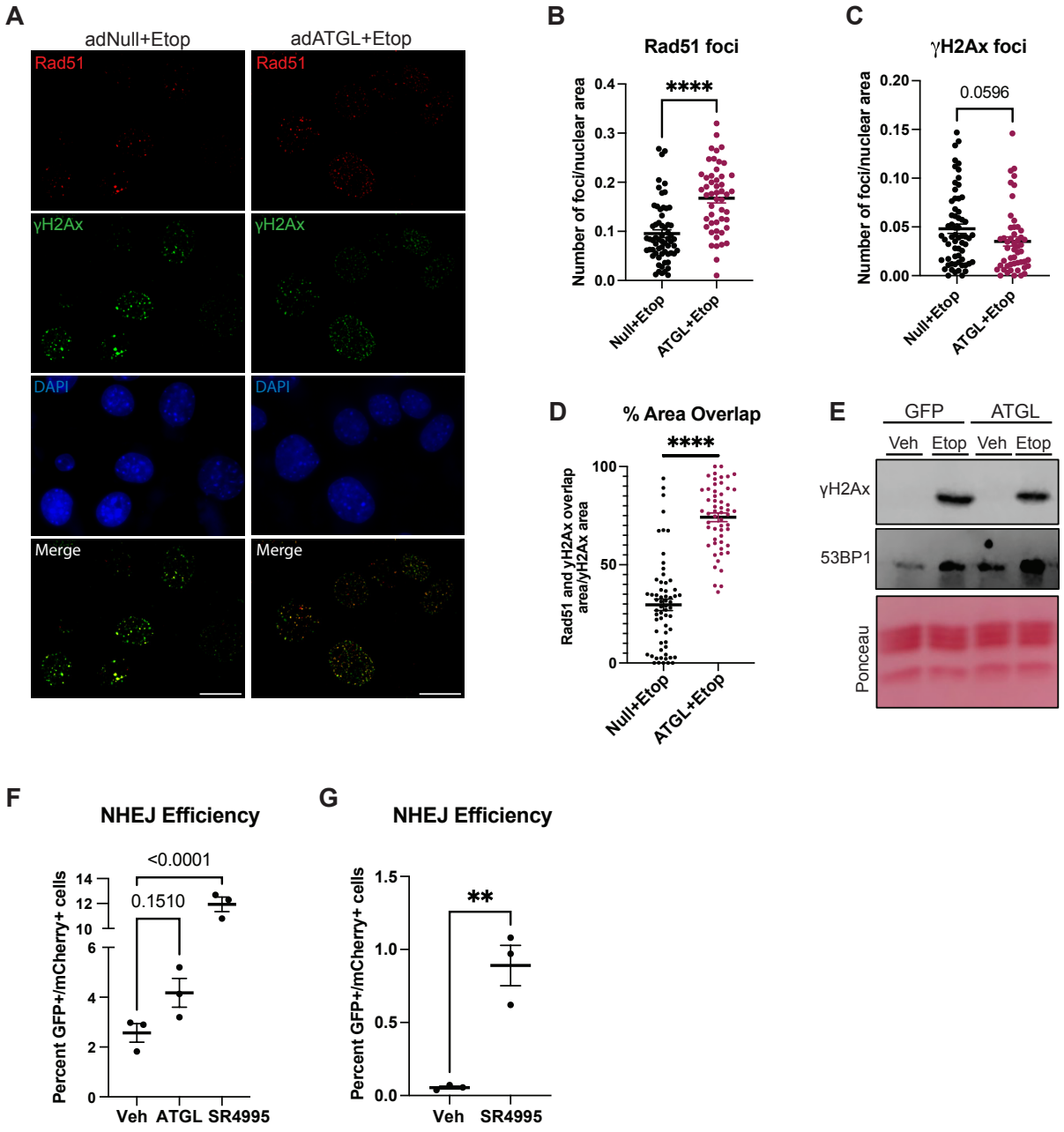

Figure 4. ATGL/lipolysis promotes DNA repair. A) AML12 cells were transduced with adNull or adATGL, treated with etoposide for 3 hours, and assayed for γH2Ax and Rad51 immunofluorescence after 24 hours of recovery. Representative images and foci number quantification per nucleus. Scale bar = 25 microns. **B)** Quantification of Rad51 foci. n=70-80. Each point on the graph represents a single nucleus. Statistics: Unpaired

t-test. ****=p<0.0001. **C)** Quantification of γH2Ax foci. Same nuclei as quantified in B (n=70-80). Statistics: Unpaired t-test. **D)** Quantification of γH2Ax/Rad51 area overlap. Percent area overlap of the cells quantified in B and C was calculated using the BIOP JACoP macro in FIJI. Statistics: Unpaired t-test. ****=p<0.0001. **E)** 53BP1 and γH2Ax immunoblot on chromatin fractions. Cells were treated with etoposide for 3 hours, then harvested and enriched for chromatin. Representative western blot of 2 independent experiments. **F)** Assessment of NHEJ repair using pimEJ5-GFP reporter that was stably transfected into AML12 cells. Statistics: one-way ANOVA with Tukey's post hoc test. Error bars on graphs indicate mean +/- SEM. **G)** Assessment of NHEJ repair using HCA2-NHEJ I9a human fibroblast cell line. Statistics: Unpaired t-test. **=p<0.005.

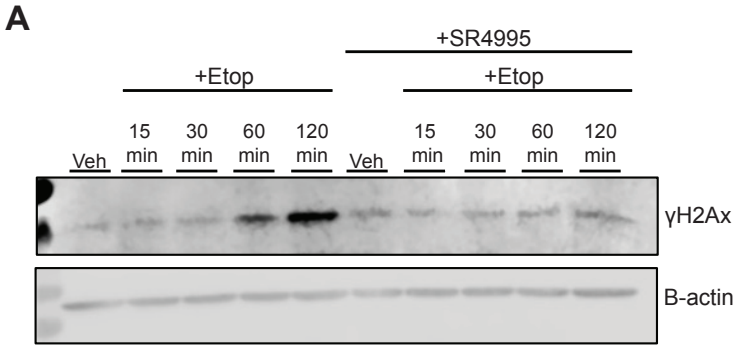

Figure 5. The effect of SR4995 on DNA damage in IMR90s. A) IMR90 cells were pre-treated with 10 μM SR-4995 for 24 hours. Etoposide was then added to cells, which were harvested at the indicated times.

ATGL/SR reduces markers of cellular senescence

Given that ATGL reduces acute DNA damage, we next asked if this translated to beneficial long-term consequences. Our lab previously showed that global overexpression of the ATGL homolog *bmm* in *Drosophila melanogaster* broadly improved multiple measures of physiological fitness and reduced markers of aging,

demonstrating enhanced locomotion, fecundity, and stress resistance.[67] As senescence is an aging hallmark, and ATGL reduces DNA damage (a senescence precursor), we hypothesized that ATGL overexpression would protect against entry into senescence. We repeatedly passaged WT and AKI Primary MEFs to induce replicative stress. At passage 6, WT MEFs had accumulated approximately 75% β-gal positive cells, while AKI MEFs of the same passage number accumulated less than half the number of senescent cells (Fig 6A). AKI MEFs also demonstrated higher 60-hour cell viability in response to high-dose etoposide (Fig 6B).

Given the robust effects of SR4995 on DNA damage (Fig 5), we chose to take advantage of this drug to modulate lipolysis in a time-dependent manner. Our models of ATGL overexpression involve either genetic overexpression or adenoviral transduction, both of which induce ATGL expression before DNA damage. Therefore, we sought to test if this protective effect on genomic stability is specific to the timing of enhanced lipolysis. To test this, we treated IMR90 cells with SR4995 before DNA damage ("SR early") or after DNA damage ("SR late") (Fig 6C). Consistent with previous experiments, SR4995-pretreated IMR90s showed reduced γH2Ax after a two-day etoposide incubation (Fig 6D). Interestingly, we observed a reduction in β-gal positive cells and cell cycle arrest markers (markers of cellular senescence) with SR4995 treatment, but only if the SR4995 was given before the DNA damage; enhancing lipolysis after DNA damage appeared to confer no benefit (Fig 6E). This data suggests that enhanced lipolysis may prime cells to better respond to genotoxic stress, but only when initiated prior to DNA damage.

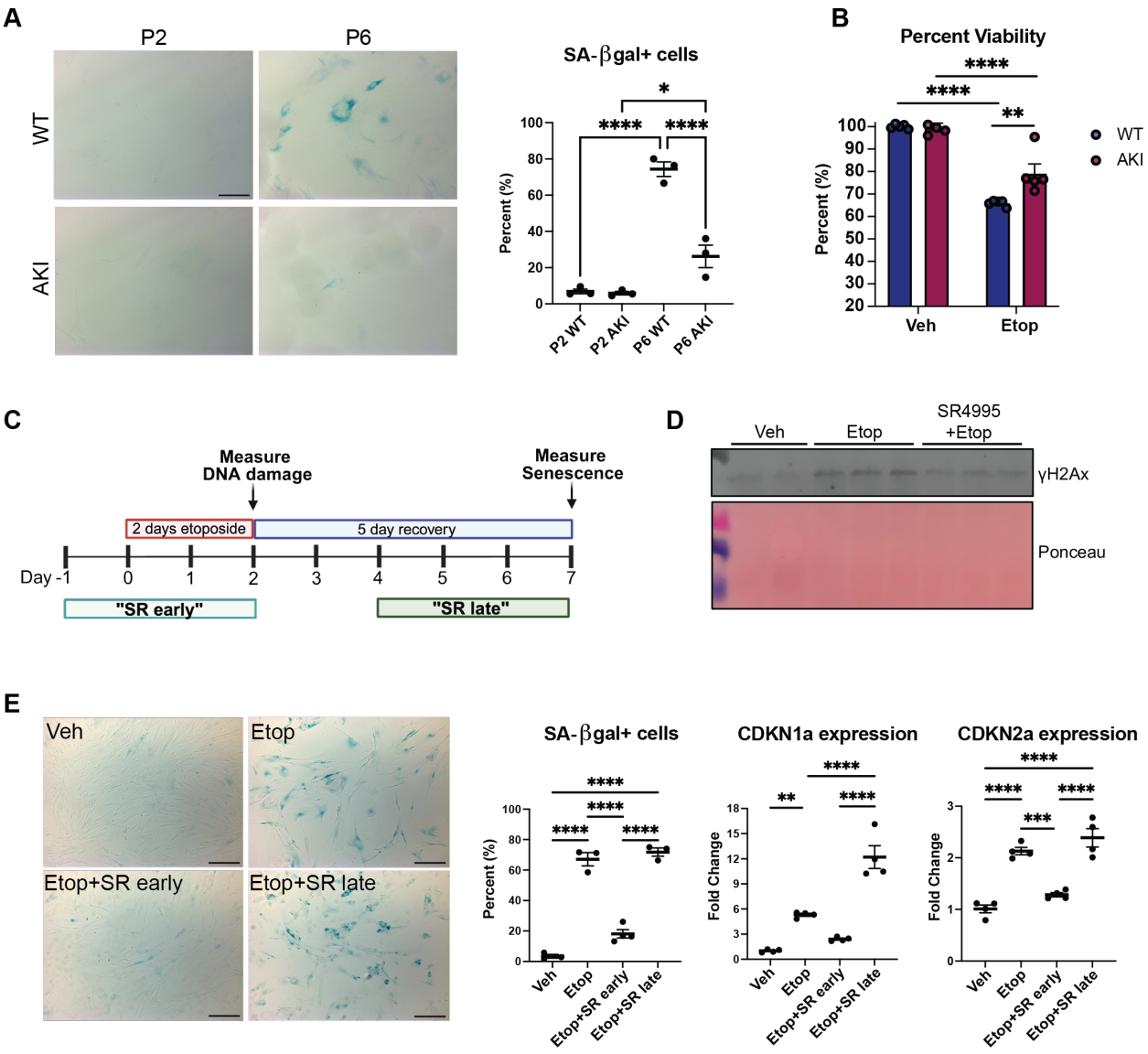

Figure 6. ATGL/lipolysis reduces markers of cellular senescence. A) Senescence-associated β-galactosidase measurement of high passage primary MEFs isolated from WT or AKI mice. Scale bar = 100 microns**.** Statistics: one-way ANOVA. *=p<0.05, ****=p<0.0001. **B)** Viability measurement of WT and AKI primary MEFs treated with 30 μM etoposide for 60 hours using the Alamar Blue assay. Statistics: one-way ANOVA with Tukey's post hoc test. **=p<0.005, ****=p<0.0001. **C)** Schematic of SR4995 timing experiment in IMR90s. **D)** γH2Ax measurement after two days of etoposide treatment. **E)** Senescence measurements denoted at the timepoint shown in (C). Scale bar = 200 microns.

ATGL KO does not increase DNA damage

Given that ATGL overexpression mitigates DNA damage, we sought to test if ATGL ablation in the opposite effect. We obtained global ATGL KO mice ("AKO") [24], which display a stark cardiac lipid accumulation that limits their lifespan and necessitates that experiments be performed on young mice. Six-week-old WT and AKO mice were irradiated with 7.5 Gy and harvested immediately after irradiation (IR acute) or after 4 hours of recovery (IR recovery). Contrary to expectations, AKO mice performed equivalently to WT mice and showed no difference in DNA damage and similar rates of γH2Ax resolution (Fig 7A). Further, AKO primary MEFs accumulate similar amounts of DNA damage as WT MEFs in response to etoposide (data not shown). Corroborating this, ATGL inhibition with ATGListatin *in vitro* resulted in no worsening of γH2Ax, suggesting ATGL is no required for DNA repair (Fig 7B).

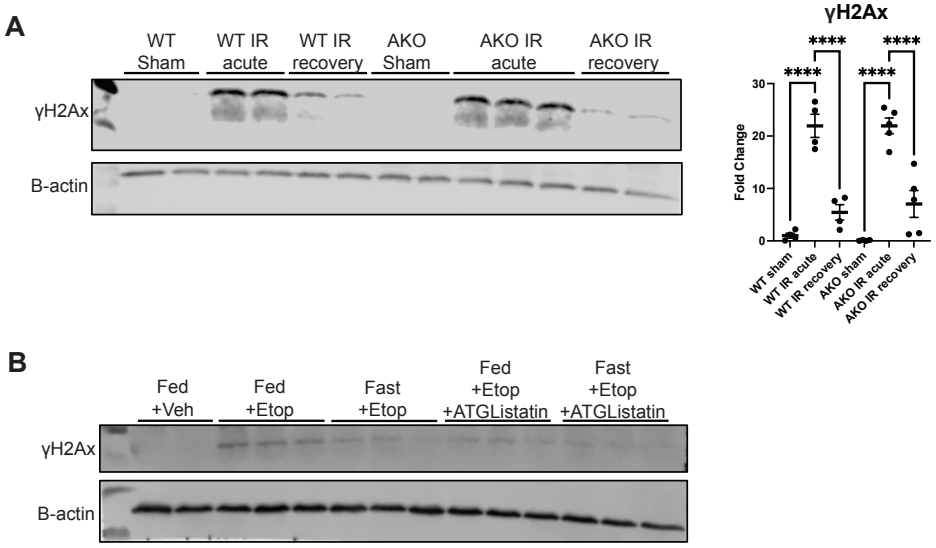

Figure 7. ATGL KO does not affect γH2Ax. A) Male ATGL KO mice of 6 weeks of age were dosed with 7.5 Gy total body irradiation and were harvested either acutely after irradiation or after 4 hours of recovery. Representative γH2Ax Western blot and quantification of all mice. n=4-5. Statistics: Two-way ANOVA. **B)** AML12 cells were

cultured in fed or fasted (1% FBS, 1 g/L glucose) media for 8 hours prior to etoposide treatment. ATGListatin treatment was given with the addition of fasting media. Cells were harvested after 3 hours of etoposide treatment.

Genotoxic stress induces LD accumulation

Our DGATi and ATGL data indicated that modulation of lipid metabolism is connected to the cell's response to DNA damage. However, the mechanisms by which DNA damage alters LD dynamics are still unclear, so we performed LD characterization in our DNA damage models. We subjected multiple cell lines to different forms of DNA damage and measured LDs by staining with BODIPY 493/503. AML12 cells and primary MEFs, liver cells and fibroblasts, respectively, both accumulate LDs with etoposide in a time-dependent manner (Fig 8A). Primary MEFs and human IMR90s are both primary cell lines capable of replicative senescence, accumulating DNA damage with repeated passages. These cells also accumulate LDs with replicative stress, indicating multiple types of damage induce LDs (Fig 8B). Of note, treatment with ATM/ATR inhibitors with etoposide still resulted in LD accumulation, indicating that LD accumulation is not dependent on acute ATM/ATR signaling (Fig 9A). Consistent with the literature, these data show that multiple cell types of human and mouse origin accumulate LDs with DNA damage.

DNA damage-induced LDs are enriched with CEs

We next sought to assess the lipid composition of damage-induced LDs. We treated WT mice with total body irradiation (7.5 Gy), harvested livers 4 hours post-IR, then fractionated LDs and performed targeted shotgun lipidomics (Fig 8C). Interestingly, purified hepatic LDs showed a stark enrichment of cholesterol esters from irradiation (Fig 8E,F). Multiple cholesterol ester species were elevated relative to sham controls, indicating multiple fatty acid chain lengths contribute to CE formation (Fig 8F). Measurement and separation of total lipids isolated from irradiated and unirradiated livers via HPLC confirmed this elevation of multiple cholesterol ester species and showed an elevation in free cholesterol (Fig 9B). Further, treatment with an ACAT (acyl-

coenzyme A cholesterol acyltransferase; esterifies cholesterol to fatty acids) inhibitor attenuated the LD accumulation with etoposide, further suggesting that the LD accumulation after DNA damage is due to cholesterol ester accumulation (Fig 8G).

Given that lipid pools were changing in irradiated livers, we sought to measure changes in lipid flux. To track fatty acid metabolites after DNA damage, we conducted pulse-chase experiments in AML12 cells, pulsing with 200 uM oleate and [^{14}C]oleate for 4 hours, followed by a chase in etoposide media. Consistent with our lab's previous work, ATGL overexpression decreased incorporation of [^{14}C]oleate into the TAG fraction during the 4-hour pulse period, likely attributable to ATGL's TAG hydrolase activity (Fig 8H). Chase data revealed a decrease in TAG 4 hours post-damage, suggesting an acute increase in lipolysis - an effect that appears to be enhanced (though not statistically significant) with ATGL overexpression (Fig 8I). After 16 hours of etoposide, increased acid-soluble metabolites (ASM) in etoposide-treated samples suggest elevated β-oxidation, despite this being the time point when we start to observe an increase in LD accumulation, consistent with a non-TAG accumulation (Fig 8A, 8J). No significant differences in cholesterol or cholesterol ester accumulation were observed (Fig 8K). Given the pool of CE is increasing with DNA damage, this could suggest the cholesterol ester accumulation is due to 1) a decrease in cholesterol ester breakdown or an increase in cholesterol ester uptake, 2) alterations in membrane remodeling resulting in cholesterol from membranes being esterified and stored in LDs, or 3) *de novo* cholesterol synthesis. Each of these possibilities would increase the CE pool without reflecting changes in flux from a labeled fatty acid. These data suggest a sequential response to DNA damage: an acute increase in lipolysis, followed by enhanced β-oxidation, and ultimately a CE-enriched lipid droplet accumulation.

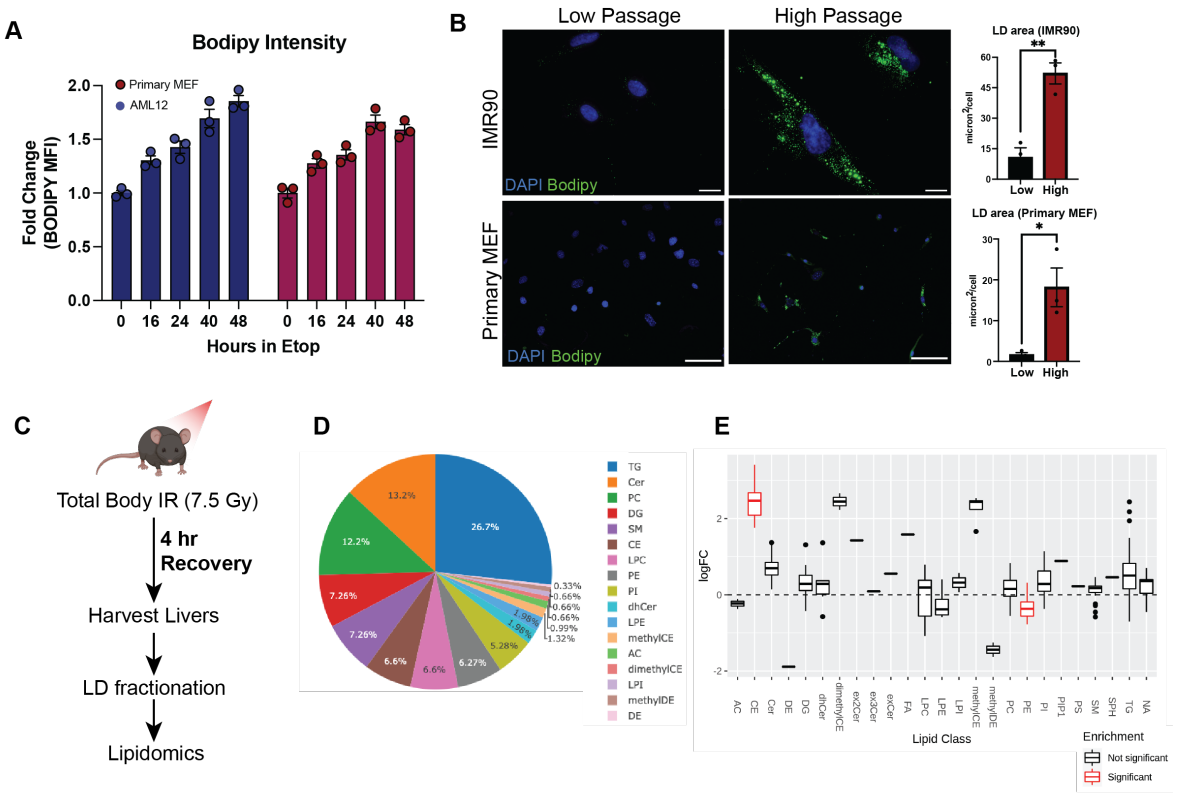
A
Bodipy Intensity
Primary MEF
AML12
Fold Change (BODIPY MFI)
Hours in Etop
B
Low Passage
High Passage
IMR90
Primary MEF
DAPI Bodipy
LD area (IMR90)
LD area (Primary MEF)
C
Total Body IR (7.5 Gy)
4 hr Recovery
Harvest Livers
LD fractionation
Lipidomics
D
E
logFC
Lipid Class
Enrichment
Not significant
Significant
F
Cholesterol Esters
Sham
IR
Fold Change
G
Veh
Etop
+DMSO
+ACATi
LD number/cell
LD number/DAPI count
Veh
Etop
ACATi
ACATi+Etop
H
TAG - Pulse
nmol/ug total protein
GFP
ATGL
I
TAG (% of Pulse TAG)
Percent (%)
4 hr
16 hr
J
ASM (%of Pulse TAG)
DPM/Pulse TG (%)
K
CE (% of total pulse)

Figure 8. LDs accumulate after genotoxic stress. A) AML12 cells and Primary MEFs were treated with 30 μM etoposide and harvested at the denoted timepoints of etoposide treatment. LDs were stained with BODIPY, and MFI was measured via flow cytometry. **B)** Primary MEFs and IMR90s were repeatedly passaged (Primary MEFs, low passage = P2, high passage = P6; IMR90, low passage = P6, high passage = P22. Primary MEF scale bar = 100 microns. IMR90 scale bar = 20 microns. A minimum of 20 cells were quantified per condition. Each point on the graph represents a condition replicate. Error bars represent mean +/- SEM. Statistics: Unpaired two-tailed t-test. ** = $p<0.005$. * = $p<0.05$. **C)** Schematic of lipidomics experiment. n=3. **D)** All detected lipid species in LD fractions that were detected over the noise ratio. Graphed by LipidSuite. **E)** Lipid classes measured as log fold change of irradiated samples relative to sham. n=3. Graphed by LipidSuite. **F)** Fold change of measured cholesterol ester species relative to sham control. **G)** AML12 cells were pretreated with 10 μM Avasimibe (ACATi) for 2 hours, then incubated in 30 μM Etoposide + Avasimibe for 24 hours. 300-600 cells quantified per condition. Each point on the graph represents a condition replicate. Error bars represent mean +/- SEM. Scale bar = 50 microns. Statistics: one-way ANOVA with Tukey's post hoc test. **=$p<0.005$, ****=$p<0.0001$. **H-K)** AML12 cells were transduced with adGFP or adATGL. 48 hours later, cells were pulsed with 200 μM oleate and [1-^{14}C]oleate for 4 hours. **H)** [1-^{14}C]oleate incorporation into cell TG during the pulse period. Etoposide was added to start the chase period. Displayed statistics are from a two-way ANOVA of all groups. All groups with multiple comparison statistics are graphed in Figure 9C. **I)** Radiolabeled TAG remaining after the 4-hour and 16-hour chase in etoposide, represented as the percent of TAG in the pulse. Statistics: two-way ANOVA. *=$p<0.05$, **=$p<0.005$. **J)** ASM from cell culture media during the 4-hour and 16-hour chase in etoposide, represented as the percent of TAG in the pulse. Statistics: two-way ANOVA. *=$p<0.05$. **K)** Radiolabeled cholesterol ester remaining after the 4-hour and 16-hour chase in etoposide, represented as the percent of total lipids in the pulse. Statistics: two-way ANOVA.

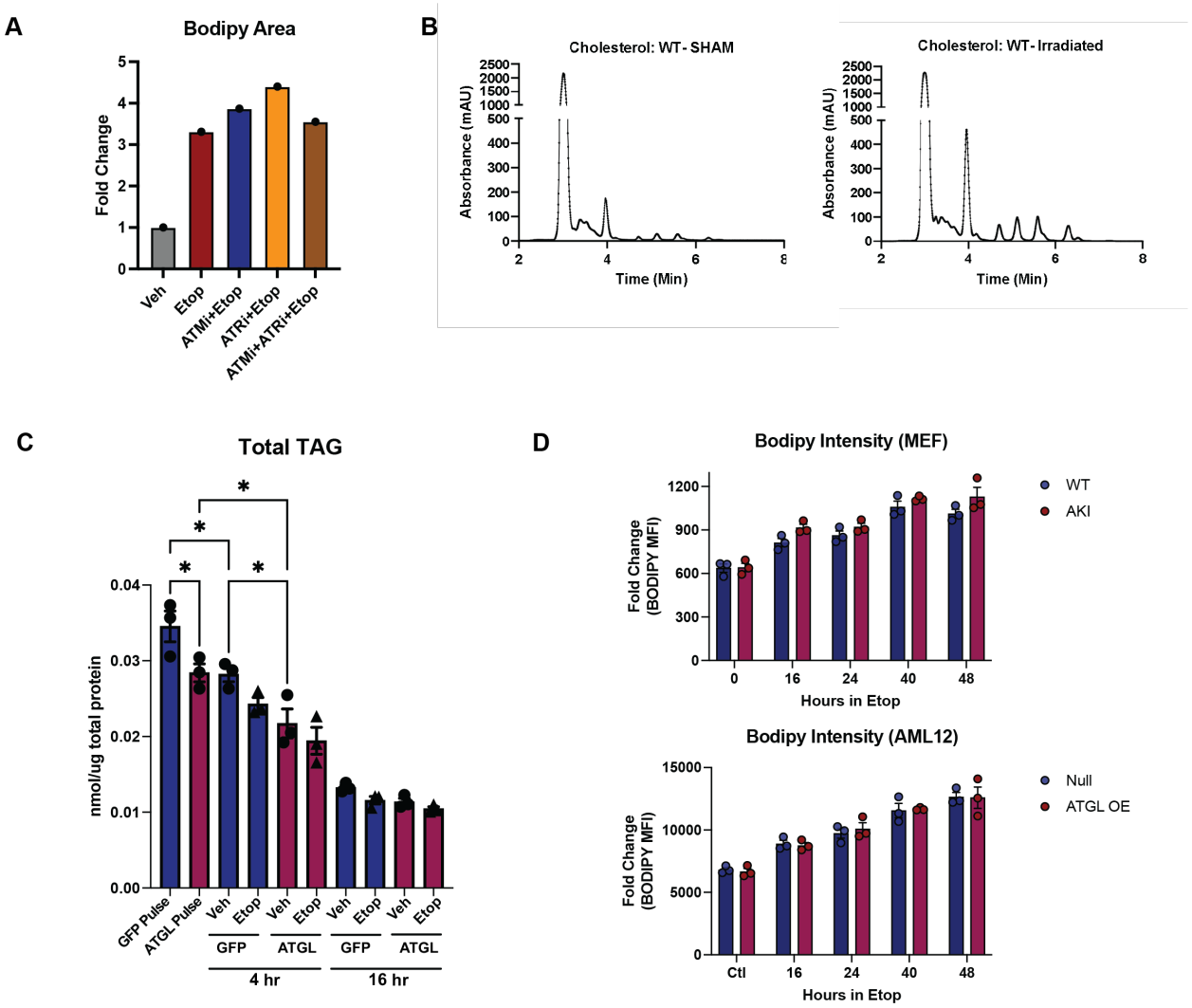

Figure 9. LDs accumulate after genotoxic stress, cont. A) LD measurement of AML12 cells pretreated with ATM or ATR inhibitor, followed by etoposide treatment for 24 hours. **B)** HPLC measurement of extracted lipids from WT mouse livers. 4-minute peak = free cholesterol. 4-7 minute peaks = presumed CE species. **C)** Measurement of total TAG normalized to total protein from pulse-chase experiment, expanded from Figure 8H. **D)** Bodipy intensity measured by flow cytometry in Primary MEFs (WT and AKI) and AML12s with and without ATGL OE.

ATGL OE does not mitigate DNA damage-induced oxidative stress

While etoposide and irradiation are robust sources of exogenous DNA damage, most of the DNA damage experienced by a cell under steady-state conditions is from endogenous sources. DNA is constantly subjected to oxidative damage by reactive oxygen species (ROS), and it is estimated that thousands of breaks can occur per cell per day as a result of ROS.[68,69] ATGL overexpression drives β-oxidation and ROS production, but also upregulates pathways to compensate and mitigate ROS.[70,71] We therefore tested if ATGL overexpression mitigated ROS under DNA damage conditions. We measured levels of mitochondrial oxidative stress in AML12 cells using a mitochondrial-targeted RX-RFP. Three hours post-irradiation, cells showed trending increases in mitochondrial oxidative stress in response to IR alone and ATGL overexpression alone, but at this acute time point, ATGL+ irradiation together drove oxidative stress (Fig 10A). Using a measure of cellular ROS (DCFDA), we corroborated that DNA damage and ATGL alone are sufficient to drive ROS acutely after etoposide (Fig 10B). Further, we measured no significant differences in 8-hydroxy-2'-deoxyguanosine (8-oxo-DG) – the most common marker of oxidative DNA damage – in irradiated livers, suggesting either that irradiation is not substantially inducing oxidative DNA damage in the liver, or that at this recovery timepoint, the amount of oxidative DNA damage is below our level of detection (Fig 10C). Altogether, these data suggest that ATGL is not mitigating ROS in the acute stages after DNA damage.

Several studies have reported that the upregulation of the PPP to support nucleotide biosynthesis is a necessary process for DNA repair.[45,47,53] While the NADPH from the PPP can support de novo lipogenesis, very few studies have looked at the inverse link – how lipolysis can promote the PPP. One study in endothelial cells shows that carbons from fatty acids can directly contribute to dNTP synthesis, while on the other hand, it was recently shown that dNTP supplementation does not rescue DNA damage after CPT1 inhibition.[50,72] Nevertheless, given that increased flux through β-oxidation can decrease reliance on glucose metabolism and potentially spare glucose for utilization by the PPP, we sought to test whether ATGL mitigated γH2Ax through the PPP. While

treatment with the glucose-6-phosphate dehydrogenase (rate-limiting step of PPP) inhibitor 6-AN worsened the DNA damage in WT etoposide-treated samples (to be expected, if nucleotide biosynthesis is stalled), 6-AN only partially mitigated the effect of ATGL overexpression and still showed a reduction in γH2Ax (Fig 10D). We repeated this with other glucose-6-phosphate dehydrogenase inhibitors and observed similar effects (data not shown). This suggests that ATGL may be partially working through increased PPP flux but is exerting other effects that lead to γH2Ax reduction.

We also chose to test how ATGL might modulate SIRT1 in the context of DNA damage. SIRT1 is heavily studied in the context of longevity and aging, and its nuclear localization and association with genomic maintenance make it an intriguing target.[73,74] Further, our lab previously showed that fatty acids derived from ATGL-mediated lipolysis lead to PLIN5 translocation from the LD to the nucleus to activate SIRT1. Given this SIRT1 activation is PLIN5-mediated, we first knocked down PLIN5 in the context of ATGL overexpression, but saw no appreciable increase in γH2Ax (Fig 10E,F). Further, we treated cells with SIRT1 inhibitor in the context of ATGL overexpression, and similar to PLIN5 KD, saw no effect on ATGL (data not shown). We took a broader approach and used nicotinamide (NAM), which acts as an inhibitor to all class III histone deacetylases (HDACs), including SIRT1. Cells treated with NAM showed no changes to γH2Ax resolution compared to untreated controls, suggesting these cells repair DNA in response to etoposide in a class III HDAC-independent mechanism (Fig 10G,H). Confirming this, we show that SIRT1 KO cells show no increase in sensitivity to etoposide (Fig 10I). Altogether, this suggests that the PLIN5-SIRT1 axis is not playing a role in DNA repair in our models.

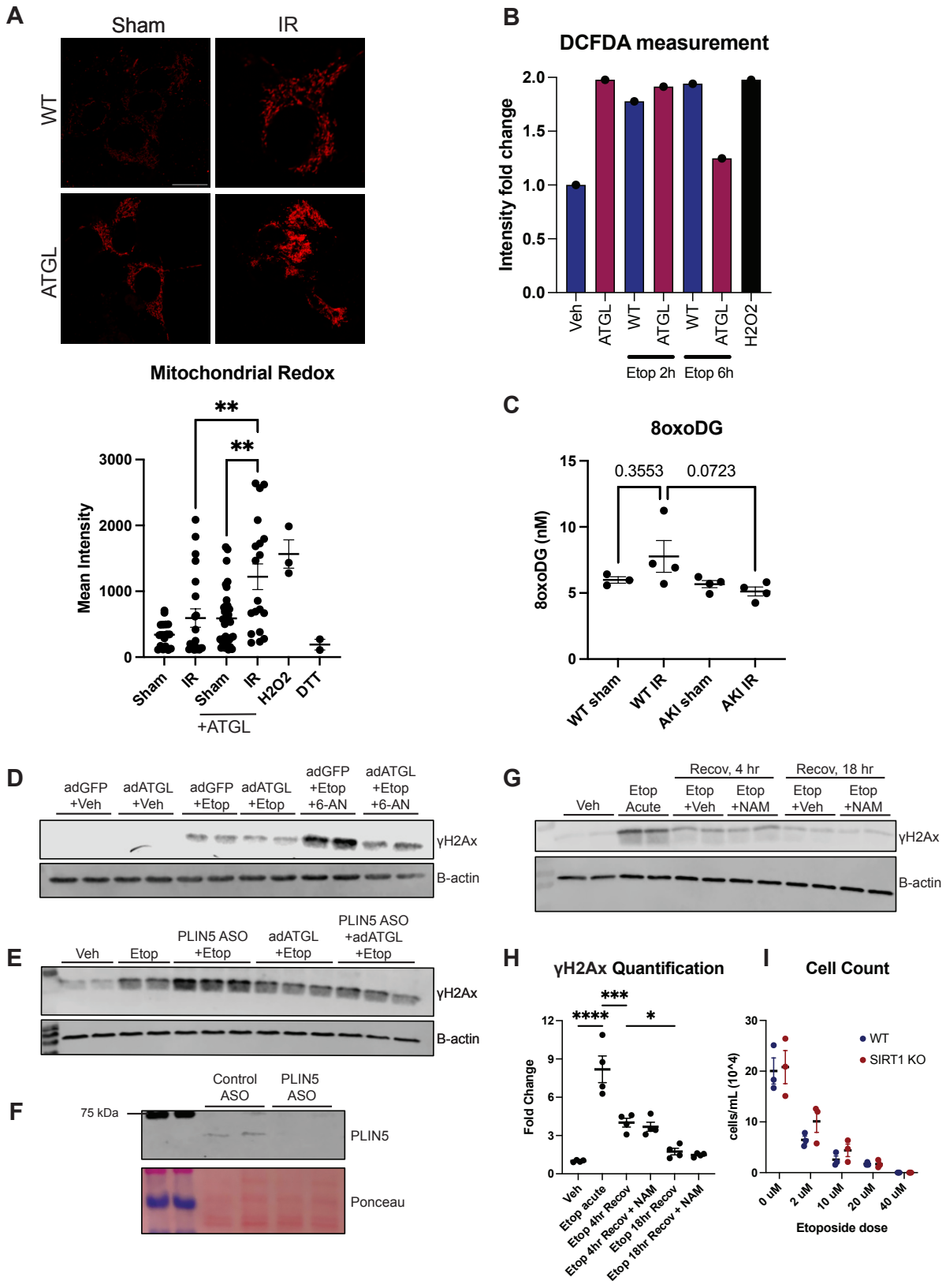
A
Sham
IR
WT
ATGL
Mitochondrial Redox
Mean Intensity
3000
2000
1000
0
**
**
Sham
IR
Sham
IR
H2O2
DTT
+ATGL
B
DCFDA measurement
Intensity fold change
2.0
1.5
1.0
0.5
0.0
Veh
ATGL
WT
ATGL
WT
ATGL
H2O2
Etop 2h
Etop 6h
C
8oxoDG
8oxoDG (nM)
15
10
5
0
0.3553
0.0723
WT sham
WT IR
AKI sham
AKI IR
D
adGFP +Veh
adATGL +Veh
adGFP +Etop
adATGL +Etop
adGFP +Etop +6-AN
adATGL +Etop +6-AN
γH2Ax
B-actin
E
Veh
Etop
PLIN5 ASO +Etop
adATGL +Etop
PLIN5 ASO +adATGL +Etop
γH2Ax
B-actin
F
Control ASO
PLIN5 ASO
75 kDa
PLIN5
Ponceau
G
Recov, 4 hr
Recov, 18 hr
Veh
Etop Acute
Etop +Veh
Etop +NAM
Etop +Veh
Etop +NAM
γH2Ax
B-actin
H
γH2Ax Quantification
Fold Change
12
9
6
3
0
****
***
*
Veh
Etop acute
Etop 4hr Recov
Etop 4hr Recov + NAM
Etop 18hr Recov
Etop 18hr Recov + NAM
I
Cell Count
cells/mL (10^4)
30
20
10
0
WT
SIRT1 KO
0 uM
2 uM
10 uM
20 uM
40 uM
Etoposide dose

Figure 10. The contribution of oxidative stress, PPP, PLIN5, and SIRT1 to DNA damage. A) Mitochondrial oxidative stress. AML12 cells were transfected with mitoRxRFP. 24 hours later, cells were transduced with ATGL. 24 hours post-transduction, cells were irradiated at 10 Gy. Cells were imaged 3 hours post-IR. Scale bar 20 microns. Statistics: one-way ANOVA with Tukey's post hoc test; ** = $p<0.05$. **B)** Whole cell ROS measurement with DCFDA (2'-7'-Dichlorodihydrofluorescein diacetate). **C)** 8-oxo-DG measurement performed on liver samples from irradiated WT and AKI mice. **D)** AML12 cells were pre-treated with PPP inhibitor 6-AN for 4 hours, followed by 3 hr etoposide treatment and 12 hours of recovery. **E)** Cells were transfected with PLIN5 ASO, followed by ATGL transduction 24 hours later. 24 hours after transduction, cells were treated with etoposide for 3 hours, followed by 12 hours of recovery. **F)** Confirmation of PLIN5 knockdown with ASO. Expected size for PLIN5 ~50 kDa. **G)** Cells were treated with etoposide, and subsequently given a 4 hour recovery or 18 hour recovery, with/without the presence of NAM. **H)** Quantification of the γH2Ax blot in G combined with another experiment (n=2 for each experiment). Statistics: one-way ANOVA with Tukey's post hoc test. *=$p<0.05$, *** = $p<0.0005$, ****=$p<0.0001$ **I)** Etoposide dose response in WT and SIRT1 KO MEFs.

<u>Chromatin acetylation state changes with ATGL overexpression</u>

A predominant cell fate for lipolyzed fatty acids is their entry into the mitochondria and subsequent β-oxidation, generating acetyl-CoA. This acetyl-CoA has several fates, largely dictated by the metabolic state of the cells; they can enter the citric acid cycle, form ketones, synthesize fatty acids/cholesterol, or acetylate proteins. Specifically, fatty acid-derived acetyl-CoA has been shown to promote both histone and non-histone protein acetylation.[75,76] Consistent with this, our data shows ATGL overexpression enhances lysine acetylation in liver lysates (Fig 11A). Irradiation also alters total acetylation, consistent with the post-translational modifications of histones and other DNA repair proteins critical for DNA repair (Fig 11A).[59]

Given that histone acetylation is essential for DNA damage detection and repair, we screened different histone acetyltransferase (HAT) inhibitors in WT and AKI Primary MEFs using γH2Ax imaging to identify if HATs are working downstream of ATGL. As expected, AKI MEFs can resolve DNA damage faster than WT MEFs, as demonstrated by a shifted γH2Ax foci distribution (Fig 11B). Of the HAT inhibitors tested, only A485 – a p300 inhibitor – abrogated the effect of ATGL on γH2Ax (Fig 11C). P300 is a well-characterized acetyltransferase in the context of DNA damage and acetylates several histone and non-histone proteins. However, we isolated histones from WT and AKI irradiated mouse livers and observed no changes in total histone acetylation state (data not shown). Though specific histone site modifications may still be occurring and just require interrogation of specific histone sites, this could suggest ATGL may enhance DNA repair through mechanisms other than broad histone acetylation.

Given that ATGL drives total lysine acetylation in the liver, that its effects are mitigated by p300 inhibition, but does not appear to be drastically increasing histone acetylation, we reasoned that ATGL could be promoting the acetylation of non-histone chromatin-bound proteins, which could promote DNA repair in these cells. We performed chromatin fractionations on AML12 cells overexpressing ATGL and observed a stark enrichment of acetylated chromatin-bound proteins with ATGL overexpression (Fig 11D). While there are moderate differences with etoposide treatment, ATGL appears to be driving the bulk of the acetyl-lysine changes. Interestingly, it appears that the most significant changes to acetylation are not happening at the expected histone molecular weights (H3–15kDa, H2A–14 kDa, H1–32 kDa), suggesting it is the non-histone chromatin-bound proteins that are being acetylated with ATGL. Given that ATGL is promoting the acetylation of chromatin-bound proteins prior to DNA damage, and that several chromatin-associated DNA repair proteins are p300 targets, this opens the doors to several possible targets as mediators of the ATGL effect on DNA repair.

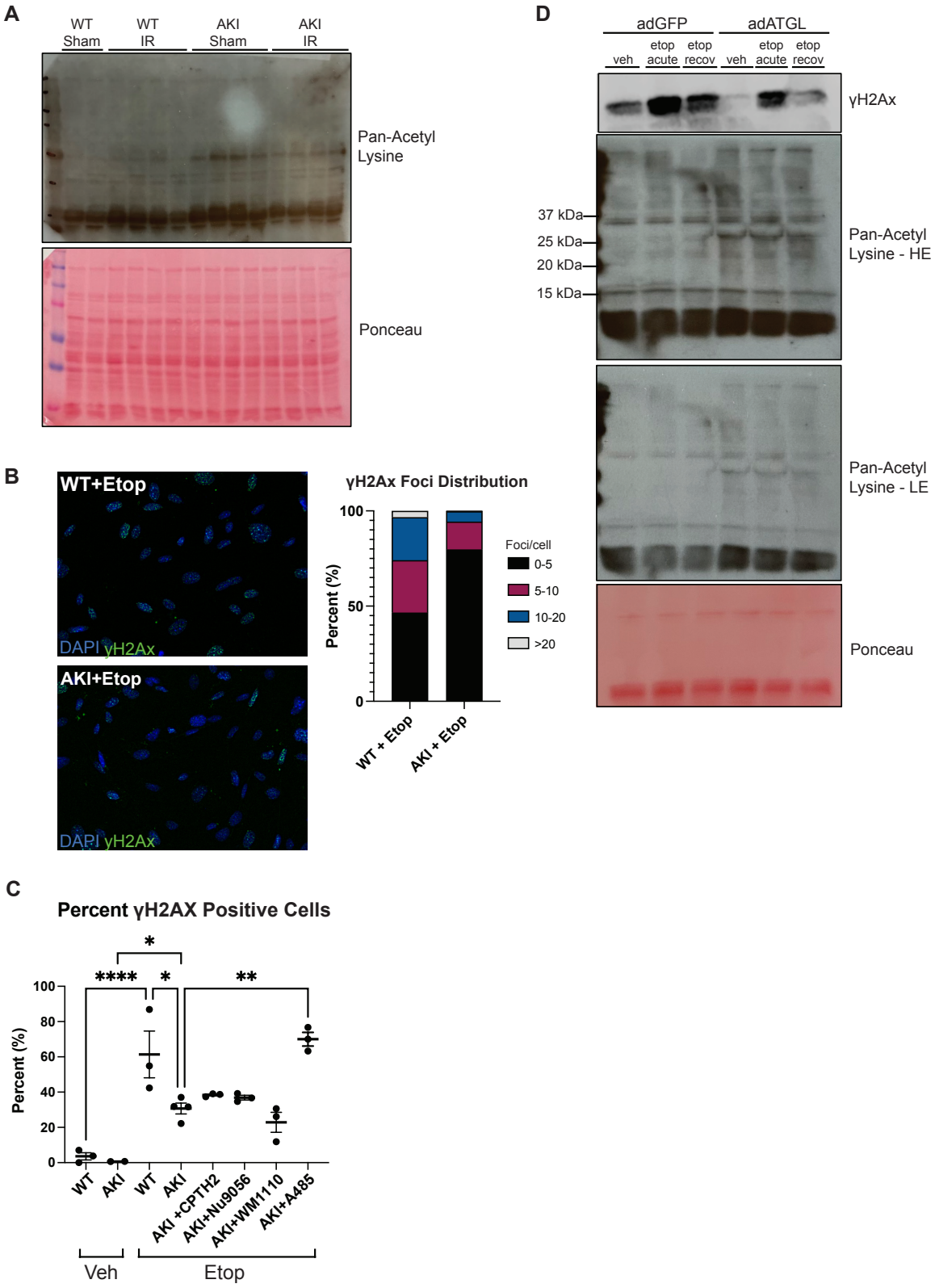
A
WT Sham
WT IR
AKI Sham
AKI IR
Pan-Acetyl Lysine
Ponceau
B
WT+Etop
DAPI γH2Ax
AKI+Etop
DAPI γH2Ax
γH2Ax Foci Distribution
Percent (%)
100
50
0
Foci/cell
0-5
5-10
10-20
>20
WT + Etop
AKI + Etop
C
Percent γH2AX Positive Cells
Percent (%)
100
80
60
40
20
0
****
*
*
**
WT
AKI
WT
AKI
AKI +CPTH2
AKI+Nu9056
AKI+WM1110
AKI+A485
Veh
Etop
D
adGFP
adATGL
veh
etop acute
etop recov
veh
etop acute
etop recov
γH2Ax
37 kDa
25 kDa
20 kDa
15 kDa
Pan-Acetyl Lysine - HE
Pan-Acetyl Lysine - LE
Ponceau

Figure 11. ATGL modulates the acetylation state. A) Immunoblotting of pan-acetyl lysine from mouse livers. **B-C)** Primary MEFs were pre-treated for 12 hours with various HAT inhibitors. Cells were then incubated in etoposide + inhibitors for 6 hours. Immunofluorescence was performed for γH2Ax, and cells were imaged using the Agilent Gen5 Cytation. **B)** Representative γH2Ax images and foci distribution. **C)** Quantification of γH2Ax positive cells (>2 foci per nucleus). Statistics: one-way ANOVA with Tukey's post hoc test. Error bars indicate mean +/- SEM. *=$p<0.05$, **=$p<0.005$, ****=$p<0.0001$. **D)** Immunoblot for γH2Ax and total acetyl-lysine on chromatin fractions isolated from GFP- or ATGL-overexpressing AML12 cells. Cells were incubated in etoposide for 3 hours ("etop acute") or allowed to recover for 3 hours after etoposide treatment ("etop recov"). HE = high exposure, LE = low exposure.

Discussion:

In this work, we identify a critical role for lipolysis in DNA repair. We show for the first time that ATGL can modulate the cell's response to DNA damage. Specifically, we show that enhancing lipolysis *before* genotoxic stress reduces DNA damage and enhances DNA repair.

While several groups have noted that FAO increases upon DNA damage, no study to date has modulated the timing of lipolysis relative to DNA damage. ATGL overexpression may precondition the cell's metabolic state prior to DNA damage by reducing glycolytic dependence while promoting β-oxidation. Indeed, it has been previously shown in a DNA damage context that ATGL overexpression reduces glucose uptake and dependence on glucose metabolism.[77] This metabolic shift could spare glucose, positioning the cells to rapidly divert carbon flux towards the PPP when DNA damage occurs. Our data suggests that PPP inhibition is required for repair of etoposide-induced damage and that this is only partly mitigated by ATGL overexpression. While this merits follow-up studies, enhanced PPP flux could be one possible mechanism through which ATGL contributes to DNA repair.

ATGL may also be priming the cell for DNA repair by increasing the total acetyl-CoA pool, thus promoting protein acetylation. We observe substantially more acetylation in the presence of ATGL in liver lysates, with notable acetylation enrichment of chromatin-bound proteins. This acetylation may facilitate DNA repair protein recruitment to chromatin, or modulate protein-protein/protein-DNA interactions that favor recruitment to damage sites.[57,78] This is consistent with our observation of enhanced localization of Rad51 and 53BP1 to the chromatin in ATGL-overexpressing cells. Inhibition of the acetyltransferase p300 completely abrogates the benefit of ATGL, suggesting one or more p300 targets are working downstream of ATGL to enhance DNA repair.
While p300 may initially suggest histones as acetylation targets, p300 also acetylates several non-histone DNA repair proteins.[79] Histone acetylation is a critical part of the

cell's response to DNA damage, but our data suggests it is the non-histone chromatin-associated proteins that are more starkly changing with ATGL (Fig 11).[59] These observations establish a foundation for future research to determine the specific proteins undergoing acetylation and to investigate whether their acetylation state mediates the effects of ATGL.

Beyond ATGL, we more broadly show a clear metabolic link between lipid droplet biology and DNA repair. We can demonstrate that LD ablation through DGAT1/2 inhibition prior to genotoxic stress increases DNA damage and promotes senescence. We also show that ATGL overexpression has no benefit in the absence of LDs. Further, we show a stark accumulation of CEs with DNA damage. Though LDs accumulate in response to several kinds of cellular stress, this accumulation is typically TAG-driven. The stark enrichment of CEs in DSB-induced LDs suggests a unique signature of DNA damage. While the CE accumulation may simply be a byproduct of the rest of the DDR, the literature suggests that the CE accumulation has functional relevance. Overjero et al. demonstrate in yeast and human cells that there is a profound sterol ester accumulation with DNA damage, and that inhibiting this accumulation reduces cell survival. They suggest that this sterol-filled LD accumulation results in sequestration of ATM, therefore tailoring the DDR and speeding up DNA repair.[80] On the other hand, Ting et al. show that cholesterol treatment in macrophages is capable of inducing DNA damage and activating PARP1.[81] While these present conflicting evidence on whether cholesterol accumulation in the context of DNA damage is beneficial or pathological, it does suggest that there is *some* role for CEs in the broader DDR process. However, this is no current evidence that the benefit of ATGL-mediated lipolysis is connected to CE accumulation. ATGL is not a known cholesterol ester hydrolase, and the presence of ATGL does not appear to mitigate the LD accumulation in AML12 cells (Fig 9D), presenting the possibility that these are distinct mechanisms that happen to converge on the LD.

The fact that perturbed ATGL function either by inhibition or knockout has no appreciable effect on γH2Ax further suggests 1) ATGL is not required for DNA repair but promotes it, and 2) that there is a larger lipid droplet dynamic at play that modulates DNA damage, as opposed to just the byproducts of ATGL-mediated lipolysis. Our ATGL knockout data suggest that ATGL is not required for mediating the cell's response to DNA damage, either *in vitro* or *in vivo* models. Recently, Markussen et al. characterized lipolysis-regulated transcriptional programs in brown adipocytes and identified gene programs that were antagonized by, required for, or sufficient in their lipolytic dependency. They show that genes that activate the DNA damage response are driven by lipolysis activation, but are not dependent on lipase activity.[82] Consistently, our ATGL overexpression model suggests that this enhanced lipolysis enhances DNA repair, but is not required for it.

Further evidence for a broader lipid droplet dynamic regulating DNA damage is the drastic reduction in γH2Ax and enhancement in NHEJ that we observe with the lipolytic activator SR4995, more so than with ATGL alone. These dramatic SR4995 findings could be explained by 1) through pharmacological activation, far more ATGL-mediated lipolytic activity is being promoted than with ATGL overexpression alone, or 2) CGI-58 is affecting something independent of ATGL to promote DNA repair. Indeed, it has been shown that there are distinct mechanisms for ATGL- and CGI-58-mediated TAG turnover in the liver, and CGI-58 can contribute to TAG turnover even in the absence of ATGL.[83] Additionally, CGI-58 can activate other lipases, alter ceramide synthesis (which is implicated in senescence induction), manipulate LD protein interactions, or alter LD dynamics in a way that supports DNA repair through mechanisms we have not yet discovered.[14,83,84]

In summary, we present the novel finding that ATGL reduces DNA damage and promotes DNA repair. We show that pharmacological activation of lipolysis further reduces DNA damage and enhances DNA repair. These findings highlight the metabolic

contribution to DNA repair and shed light on a novel mechanism by which lipid metabolism enhances genomic stability.

Chapter 3:

Future Directions

While we show for the first time that ATGL can modulate DNA damage and repair, the question of how ATGL mitigates DNA damage remains our active area of pursuit. We have ruled out several hypotheses and have shed light on new ones. Our main areas of future investigation will focus on 1) the role of ATGL in metabolic regulation prior to DNA damage, 2) the role of other LD proteins in regulating DNA repair, and 3) the role of ATGL-driven acetylation in regulating the DNA damage response.

The role of ATGL in metabolic regulation prior to DNA damage

The time dependence of lipolysis activation has directed our focus towards cellular conditions downstream of ATGL that prime the cell to better respond to DNA damage. The DDR is an energetically demanding process – the ATP-consuming reactions by upstream DDR kinases accompanied by the dramatic NAD+ depletion by enzymes like PARP-1 may require the upregulation of catabolic pathways like lipolysis and FAO for cell survival, especially in the context of glycolysis downregulation.[49] A few studies report that an increase in FAO post-DNA damage is critical for damage control and cell survival, with one study suggesting β-oxidation is required to meet the energy demands of DNA repair.[50,51] While ATGL overexpression promotes FAO, supporting this mechanism of energy repletion, this conflicts with the observation that ATGL KO has no discernible effect on DNA damage. If ATP were limiting and dependent on ATGL-mediated lipolysis and subsequent FAO, ATGL inhibition would result in increased DNA damage or cell death. While we have not ruled out an ATP-mediated effect of ATGL, in most of our models of DNA damage, non-ATGL overexpressing cells still survive the insult, suggesting they are not in an energy crisis leading to apoptosis. Further, the stark cholesterol ester accumulation suggests de novo cholesterol synthesis – an ATP-requiring process – that argues against an energy deficiency at the levels of DNA damage we are inducing.

While we have shown that ATGL enhances lipolysis in the context of DNA damage, we are still investigating if the metabolic consequences of this are directly responsible for the mitigation of DNA damage. ATGL overexpression may shift the cell's metabolic

state before DNA damage by reducing glycolytic dependence while promoting PPP, and our preliminary data suggest that PPP inhibition, at least in part, mitigates the effect of ATGL. However, several reasons exist for not seeing a complete rescue of the ATGL phenotype. First, it is possible that nucleotide biosynthesis is not rate-limiting for the repair with the amount of DNA damage we are inducing. This logic can also be applied to oxidative stress – the NADPH produced by the PPP may not be fully limiting in our models of DNA damage, and ATGL plays no contributory role in mitigating oxidative stress in these contexts. However, Jeong et al. showed that glutamine is redirected from an anaplerotic fate towards nucleotide biosynthesis during DNA damage – cell culture media is often, and in our case, glutamine-supplemented, which could potentially be masking the effect of the PPP dependence of ATGL-mediated repair.[53] While several studies are required to test this hypothesis (i.e., PPP inhibition in glutamine-free media, measurement of PPP metabolite pools, PPP flux measurements, nucleotide supplementation, or NADPH/ROS scavenger supplementation), this could be one possible mechanism through which ATGL contributes to DNA repair.

We are also investigating the metabolic origins and consequences of the stark CE accumulation following DNA damage. The β-oxidation following DNA damage generates acetyl-CoA that could fuel cholesterol synthesis, further supported by increased NADPH from the PPP. Our pulse-chase data suggest that CE accumulation is not due to rapid esterification with oleate, and that the source of damage-induced CE does not originate from TAGs. This argues for *de novo* cholesterol synthesis, which is under the regulatory control of the Sterol Regulatory Element-Binding Proteins (SREBPs). HMG-CoA reductase catalyzes the rate-limiting step of cholesterol biosynthesis and is under SREBP control. As for the possible mechanisms leading to increased SREBP signaling, we observe increased ROS with DNA damage (and with ATGL overexpression); this increased ROS has also been shown to promote SREBP activity.[85,86] Additionally, PARP-1, which is highly active in states of DNA damage, is responsive to oxysterols and can modulate lipid signaling pathways like PPARα, which has been shown to direct cholesterol efflux and cholesterol esterification.[81,87–89] Further experiments, such as

tracing experiments with labeled cholesterol and investigation of upstream cholesterol signaling (SREBP, etc.), will help to elucidate the origin of this CE accumulation. While we do not currently have evidence that the benefit of ATGL-mediated lipolysis is connected to CE accumulation, we are actively testing the role of cholesterol esterification and measuring LD composition changes in our models. ATGL is not a known cholesterol ester hydrolase, and the presence of ATGL does not appear to mitigate the LD accumulation in AML12 cells (Fig 9D), presenting the possibility that these are distinct mechanisms that happen to converge on the LD. The connections between CE and DNA repair, and between ATGL and CE, remain open.

The role of other LD proteins in DNA repair

Beyond ATGL, we show potential roles for DGAT1/2 and CGI-58 in DNA damage. We show that LD ablation through DGAT1/2 inhibition prior to genotoxic stress increases DNA damage and promotes senescence. There are several consequences of DGAT inhibition; first, there is a dramatic reduction in TAG synthesis, functionally resulting in LD ablation. There is also a resultant increase in DAGs and unesterified fatty acids, which have the potential to accumulate or be redirected towards other metabolites. DAG accumulation can cause ER stress and lipotoxicity, and though we confirmed DGAT1/2 inhibition alone was not causing DNA damage, it is possible that it could cause damage combined with the oxidative stress of etoposide through a lipid peroxidation mechanism. It is also possible that the enhanced damage with DGAT inhibition sheds light on the CE phenotype. For instance, we observe more dramatic effects of DGAT inhibition in IMR90 fibroblasts over AML12 hepatocytes (Fig 1C, Fig 2F). DGAT inhibition in some cells has been shown to ablate all LD formation, but in other cells, DGAT inhibition still allows for CE-rich LDs to form.[90] IMR90s do not accumulate LDs with Etoposide+DGAT1/2 inhibition, but AML12 cells may still have the capacity to store CE despite DGAT1/2 inhibition. Given our observation that CE accumulates with DNA damage, it is possible that this CE accumulation is part of the DNA damage response, and its accumulation in AML12s is sufficient to mitigate the worsened DNA damage phenotype.

The stark improvement in DNA damage and DNA repair with SR4995 suggests an enhanced efficacy over ATGL overexpression alone. While SR4995 can increase ATGL-catalyzed lipolysis by promoting CGI-58 dissociation from PLINs, CGI-58 could be modulating pathways independent of ATGL to promote DNA repair. CGI-58 is more than an ATGL activator – it can activate other lipases, alter ceramide synthesis (which is implicated in senescence induction), manipulate LD protein interactions, or alter LD dynamics in a way that supports DNA repair through mechanisms we have not yet discovered.[14,83,84] Further, mutations in CGI-58 have a unique phenotype *in vivo* beyond what is seen with ATGL mutations, suggesting its ATGL-independent effects may affect critical processes, potentially including DNA repair.[15] Our first objective is to test if ATGL knockout mitigates the effects of SR4995 to test if ATGL is working downstream of SR4995. Subsequently, we can investigate if CGI-58 overexpression alone can mitigate DNA damage. This could reveal a completely new dimension to CGI-58, ATGL regulation, and the role of LD proteins in DNA repair.

<u>The role of ATGL-driven acetylation</u>

Our data suggests that chromatin-bound proteins are increasing in acetylation state with ATGL overexpression. While there are several non-histone proteins bound to the chromatin, we can narrow our focus to known p300 targets. For instance, PARP-1 presents an intriguing target for us. PARP-1 responds directly to several kinds of DNA breaks, binding directly to DNA and catalyzing poly-ADP-ribosylation (PARylation) of a variety of targets in a NAD+-dependent manner, thus playing a vital role in DNA repair. Intriguingly, PARP-1 is connected to nearly every proposed mechanism described here – not only does it play a critical role in DNA damage/repair, it is connected to cholesterol metabolism, it promotes β-oxidation and inhibits glycolysis in response to DNA damage, it can be activated by FAO, is responsive to oxidative stress, and its acetylation state can modulate chromatin association and DNA repair.[49,50,91,92] Finally, PARP-1 can be acetylated by p300, the singular target of our HAT inhibitor screen, suggesting that PARP-1 could be playing a role in modulating the phenotype of ATGL in Primary MEFs (Figure 11B,C).[93] Given the notable connection between PARP-1 dynamics, LD

metabolism, and DNA repair, we are actively investigating its potential roles downstream of ATGL.

Further, it is well-known that acetylation of chromatin can vastly affect chromatin accessibility to transcription factors. To assess pathways that may be upregulated with ATGL, we are pursuing RNA sequencing in livers of ATGL overexpression mice with and without IR. Chromatin is not simply structural; it plays an active role in sensing, detection, protein recruitment, nuclear partitioning, and repair of DNA damage.[57] Given that ATGL is increasing acetylation of chromatin, it may also more broadly affect chromatin dynamics, which would be a completely novel dimension of ATGL-mediated activity. Future exploration of chromatin accessibility, dynamics, and integration presents promising avenues for investigation.

Implications for aging, cancer, and more

Finally, it is well-established that alterations in lipid metabolism are common phenotypes observed with aging and senescence.[37,38,61,84] While we have studied ATGL primarily in the context of acute DNA damage, unrepaired DNA damage drives genomic instability, the main precursor to senescence and age-related disease. We show that ATGL/enhanced lipolysis can reduce senescence markers (Fig 6), and as a result, this work has greater implications beyond acute exogenous genotoxic stress. By manipulating lipolysis in a healthy or acutely damaged cell, perhaps it is possible to divert the senescence fate and encourage DNA repair.

Fasting and caloric restriction – metabolic states that upregulate ATGL and lipolysis – are potent modulators of lifespan and enhancers of healthspan. One of the key responses to fasting is the upregulation of lipolysis to preserve energy balance. Our data suggests that mechanisms downstream of fasting (lipolysis, β-oxidation) prime cells to mitigate DNA damage, therefore presenting a possible mechanism through which fasting and lipolysis enhance genomic stability and healthspan. Understanding

the mechanisms by which fasting promotes healthspan opens the door for the development of pharmacological targets to activate these pathways.

This work has particularly strong implications in populations undergoing chronic DNA damage. For instance, chemotherapeutic drugs are most often DNA-damaging agents intended to kill malignant cells, but often have off-target effects. However, more studies are beginning to show that fasting protects mice from lethal levels of DNA damage.[94] More data is also emerging suggesting that fasting not only has a cytoprotective effect, but also has a synergistic cytotoxic effect against cancer cells. Data from several studies suggest that fasting sensitizes cancer cells to chemotherapy while protecting non-cancerous cells. For instance, mice with pancreatic tumors that receive a fasting regimen and irradiation combination have dramatically increased survival and delayed tumor progression relative to fed tumor-bearing mice.[95,96] This suggests that fasting prior to chemotherapy (or targeted pharmacological manipulation of these pathways) could potentially upregulate DNA repair mechanisms and protect against off-target effects of chemotherapy. Finally, ATGL has been shown to mediate the effect of dietary restriction on longevity, suggesting that at least one mechanism through which fasting is beneficial is through lipolytic activity.[97]

This work has been able to set the foundation for a brand-new area of study for our group. By connecting lipid catabolism and DNA repair, we have been able to highlight the metabolic contribution to DNA repair, of which very little is known outside of nucleotide metabolism. This opens the door for several exciting directions as we further explore how ATGL and lipid metabolism drive genomic stability.

References:

1. Prorok P, Grin IR, Matkarimov BT, Ishchenko AA, Laval J, Zharkov DO, Saparbaev M. Evolutionary Origins of DNA Repair Pathways: Role of Oxygen Catastrophe in the Emergence of DNA Glycosylases. Cells. 10(7),1591, (2021).
2. Bhogal, N., Jalali, F. & Bristow, R. G. Microscopic imaging of DNA repair foci in irradiated normal tissues. *Int. J. Radiat. Biol.* **85**, 732–746 (2009).
3. Podhorecka, M., Skladanowski, A. & Bozko, P. H2AX Phosphorylation: Its Role in DNA Damage Response and Cancer Therapy. *J. Nucleic Acids* **2010**, 920161 (2010).
4. Celeste, A. *et al.* Genomic Instability in Mice Lacking Histone H2AX. *Science* **296**, 922–927 (2002).
5. Clay, D. E. & Fox, D. T. DNA Damage Responses during the Cell Cycle: Insights from Model Organisms and Beyond. *Genes* **12**, 1882 (2021).
6. Cary, R. B. *et al.* DNA looping by Ku and the DNA-dependent protein kinase. *Proc Natl Acad Sci* (1997) doi:10.1073/pnas.94.9.4267.
7. Liu, S. & Kong, D. End resection: a key step in homologous recombination and DNA double-strand break repair. *Genome Instab. Dis.* **2**, 39–50 (2021).
8. Ahel, D. *et al.* Poly(ADP-ribose)–Dependent Regulation of DNA Repair by the Chromatin Remodeling Enzyme ALC1. *Science* **325**, 1240–1243 (2009).
9. Polo, S. E. & Jackson, S. P. Dynamics of DNA damage response proteins at DNA breaks: a focus on protein modifications. *Genes Dev.* **25**, 409–433 (2011).
10. López-Otín, C., Blasco, M. A., Partridge, L., Serrano, M. & Kroemer, G. Hallmarks of aging: An expanding universe. *Cell* **186**, 243–278 (2023).

11. Olzmann, J. A. & Carvalho, P. Dynamics and functions of lipid droplets. *Nat. Rev. Mol. Cell Biol.* **20**, 137–155 (2019).

12. Najt, C. P., Devarajan, M. & Mashek, D. G. Perilipins at a glance. *J. Cell Sci.* **135**, jcs259501 (2022).

13. Bersuker, K. *et al.* A Proximity Labeling Strategy Provides Insights into the Composition and Dynamics of Lipid Droplet Proteomes. *Dev. Cell* **44**, 97-112.e7 (2018).

14. Brown, A. L. & Mark Brown, J. Critical roles for α/β hydrolase domain 5 (ABHD5)/comparative gene identification-58 (CGI-58) at the lipid droplet interface and beyond. *Biochim. Biophys. Acta BBA - Mol. Cell Biol. Lipids* **1862**, 1233–1241 (2017).

15. Lefèvre, C. *et al.* Mutations in CGI-58, the Gene Encoding a New Protein of the Esterase/Lipase/Thioesterase Subfamily, in Chanarin-Dorfman Syndrome. *Am. J. Hum. Genet.* **69**, 1002–1012 (2001).

16. Lass, A. *et al.* Adipose triglyceride lipase-mediated lipolysis of cellular fat stores is activated by CGI-58 and defective in Chanarin-Dorfman Syndrome. *Cell Metab.* **3**, 309–319 (2006).

17. Cerk, I. K., Wechselberger, L. & Oberer, M. Adipose Triglyceride Lipase Regulation: An Overview. *Curr Protein Pept Sci* **19**, 221–233 (2018).

17. Listenberger, L. L., Ostermeyer-Fay, A. G., Goldberg, E. B., Brown, W. J., & Brown, D. A. Adipocyte differentiation-related protein reduces the lipid droplet association of adipose triglyceride lipase and slows triacylglycerol turnover. *Journal of lipid research. 48*(12), 2751–2761 (2007).

19. Kim, J. Y., Tillison, K., Lee, J.-H., Rearick, D. A. & Smas, C. M. The adipose tissue triglyceride lipase ATGL/PNPLA2 is downregulated by insulin and TNF-α in 3T3-L1 adipocytes and is a target for transactivation by PPARγ. *Am. J. Physiol.-Endocrinol. Metab.* **291**, E115–E127 (2006).

20. Chakrabarti, P. & Kandror, K. V. FoxO1 Controls Insulin-dependent Adipose Triglyceride Lipase (ATGL) Expression and Lipolysis in Adipocytes. *J. Biol. Chem.* **284**, 13296–13300 (2009).

21. Schweiger, M. *et al.* The C-terminal Region of Human Adipose Triglyceride Lipase Affects Enzyme Activity and Lipid Droplet Binding. *J. Biol. Chem.* **283**, 17211–17220 (2008).

22. Lulić, A.-M. & Katalinić, M. The PNPLA family of enzymes: characterisation and biological role. *Arch. Ind. Hyg. Toxicol.* **74**, 75–89 (2023).

23. Kohlmayr, J. M. *et al.* Mutational scanning pinpoints distinct binding sites of key ATGL regulators in lipolysis. *Nat. Commun.* **15**, 2516 (2024).

24. Haemmerle, G. *et al.* Defective Lipolysis and Altered Energy Metabolism in Mice Lacking Adipose Triglyceride Lipase. *Science* **312**, 734–737 (2006).

25. Smirnova, E. *et al.* ATGL has a key role in lipid droplet/adiposome degradation in mammalian cells. *EMBO Rep.* **7**, 106–113 (2006).

26. Ahmadian, M. *et al.* Adipose Overexpression of Desnutrin Promotes Fatty Acid Use and Attenuates Diet-Induced Obesity. *Diabetes* **58**, 855–866 (2009).

27. Schreiber, R., Xie, H. & Schweiger, M. Of mice and men: The physiological role of adipose triglyceride lipase (ATGL). *Biochim. Biophys. Acta BBA - Mol. Cell Biol. Lipids* **1864**, 880–899 (2019).

28. Ong, K. T., Mashek, M. T., Bu, S. Y., Greenberg, A. S. & Mashek, D. G. Adipose triglyceride lipase is a major hepatic lipase that regulates triacylglycerol turnover and fatty acid signaling and partitioning. *Hepatology* **53**, 116–126 (2011).

28. Taschler, U., Schreiber, R., Chitraju, C., Grabner, G. F., Romauch, M., Wolinski, H., Haemmerle, G., Breinbauer, R., Zechner, R., Lass, A., & Zimmermann, R. Adipose triglyceride lipase is involved in the mobilization of triglyceride and retinoid stores of hepatic stellate cells. *Biochimica et biophysica acta*, *1851*(7), 937–945, (2015).

30. Patel, R. *et al.* ATGL is a biosynthetic enzyme for fatty acid esters of hydroxy fatty acids. *Nature* **606**, 968–975 (2022).

31. Notari, L. *et al.* Identification of a Lipase-linked Cell Membrane Receptor for Pigment Epithelium-derived Factor. *J. Biol. Chem.* **281**, 38022–38037 (2006).

32. Li, W. *et al.* Adipose triglyceride lipase suppresses noncanonical inflammasome by hydrolyzing LPS. *Nat. Chem. Biol.* **20**, 1434–1442 (2024).

33. Khatchadourian, A., Bourque, S. D., Richard, V. R., Titorenko, V. I. & Maysinger, D. Dynamics and regulation of lipid droplet formation in lipopolysaccharide (LPS)-stimulated microglia. *Biochim. Biophys. Acta BBA - Mol. Cell Biol. Lipids* **1821**, 607–617 (2012).

34. Welte, M. A. & Gould, A. P. Lipid droplet functions beyond energy storage. *Biochim. Biophys. Acta BBA - Mol. Cell Biol. Lipids* **1862**, 1260–1272 (2017).

35. Smolič, T. *et al.* Astrocytes in stress accumulate lipid droplets. *Glia* **69**, 1540–1562 (2021).

36. Henne, W. M., Reese, M. L. & Goodman, J. M. The assembly of lipid droplets and their roles in challenged cells. *EMBO J.* **37**, e98947 (2018).

37. Russo, T. & Riessland, M. Lipid accumulation drives cellular senescence in dopaminergic neurons. *Aging* **16**, 11128–11133 (2024).

38. Ogrodnik, M. *et al.* Obesity-Induced Cellular Senescence Drives Anxiety and Impairs Neurogenesis. *Cell Metab.* **29**, 1061-1077.e8 (2019).

39. Xu, S. & Offermanns, S. Endothelial lipid droplets drive atherosclerosis and arterial hypertension. *Trends Endocrinol. Metab.* **35**, 453–455 (2024).

40. Teixeira, L. *et al.* Prevention of lipid droplet accumulation by DGAT1 inhibition ameliorates sepsis-induced liver injury and inflammation. *JHEP Rep.* **6**, 100984 (2024).

41. Villanueva, C. J. *et al.* Specific role for acyl CoA: Diacylglycerol acyltransferase 1 (Dgat1) in hepatic steatosis due to exogenous fatty acids†. *Hepatology* **50**, 434–442 (2009).

42. Perilipin-2-null mice are protected against diet-induced obesity, adipose inflammation, and fatty liver disease[S] - PIIS0022227520421728.

43. Listenberger, L. L. *et al.* Triglyceride accumulation protects against fatty acid-induced lipotoxicity. *Proc. Natl. Acad. Sci.* **100**, 3077–3082 (2003).

44. Herms, A. *et al.* Cell-to-Cell Heterogeneity in Lipid Droplets Suggests a Mechanism to Reduce Lipotoxicity. *Curr. Biol.* **23**, 1489–1496 (2013).

45. Cosentino, C., Grieco, D. & Costanzo, V. ATM activates the pentose phosphate pathway promoting anti-oxidant defence and DNA repair: ATM activates the pentose phosphate pathway. *EMBO J.* **30**, 546–555 (2011).

46. Juvekar, A. *et al.* Phosphoinositide 3-kinase inhibitors induce DNA damage through nucleoside depletion. *Proc. Natl. Acad. Sci.* **113**, (2016).

47. Milanese, C. *et al.* DNA damage and transcription stress cause ATP-mediated redesign of metabolism and potentiation of anti-oxidant buffering. *Nat. Commun.* **10**, 4887 (2019).

47. Andrabi, S. A., Umanah, G. K., Chang, C., Stevens, D. A., Karuppagounder, S. S., Gagné, J. P., Poirier, G. G., Dawson, V. L., & Dawson, T. M. Poly(ADP-ribose) polymerase-dependent energy depletion occurs through inhibition of glycolysis. *Proceedings of the National Academy of Sciences of the United States of America*, *111*(28), 10209–10214 (2014).

49. Murata, M. M. *et al.* NAD+ consumption by PARP1 in response to DNA damage triggers metabolic shift critical for damaged cell survival. *Mol. Biol. Cell* **30**, 2584–2597 (2019).

50. Yang, S. *et al.* Fatty acid oxidation facilitates DNA double-strand break repair by promoting PARP1 acetylation. *Cell Death Dis.* **14**, 435 (2023).

51. Brace, L. E. *et al.* Increased oxidative phosphorylation in response to acute and chronic DNA damage. *Npj Aging Mech. Dis.* **2**, 16022 (2016).

52. Assaily, W. *et al.* ROS-Mediated p53 Induction of Lpin1 Regulates Fatty Acid Oxidation in Response to Nutritional Stress. *Mol. Cell* **44**, 491–501 (2011).

53. Jeong, S. M. *et al.* SIRT4 Has Tumor-Suppressive Activity and Regulates the Cellular Metabolic Response to DNA Damage by Inhibiting Mitochondrial Glutamine Metabolism. *Cancer Cell* **23**, 450–463 (2013).

54. Goudarzi, M. *et al.* The effect of low dose rate on metabolomic response to radiation in mice. *Radiat. Environ. Biophys.* **53**, 645–657 (2014).

55. Laiakis, E. C. *et al.* Development of a Metabolomic Radiation Signature in Urine from Patients Undergoing Total Body Irradiation. *Radiat. Res.* **181**, 350 (2014).

56. Yang, S., Moon, S., Hur, S. C. & Jeong, S. M. Fatty acid oxidation regulates cellular senescence by modulating the autophagy-SIRT1 axis. *BMB Rep.* **56**, 651–656 (2023).

57. Aricthota, S., Rana, P. P. & Haldar, D. Histone acetylation dynamics in repair of DNA double-strand breaks. *Front. Genet.* **13**, 926577 (2022).

58. McDonnell, E. *et al.* Lipids Reprogram Metabolism to Become a Major Carbon Source for Histone Acetylation. *Cell Rep.* **17**, 1463–1472 (2016).

59. Sivanand, S. *et al.* Nuclear Acetyl-CoA Production by ACLY Promotes Homologous Recombination. *Mol. Cell* **67**, 252-265.e6 (2017).

60. Yamauchi, S. *et al.* Mitochondrial fatty acid oxidation drives senescence. *Sci. Adv.* **10**, eado5887 (2024).

61. Hamsanathan, S. *et al.* Integrated -omics approach reveals persistent DNA damage rewires lipid metabolism and histone hyperacetylation via MYS-1/Tip60. *Sci. Adv.* **8**, eabl6083 (2022).

62. Fuhrmann-Stroissnigg, H. *et al.* SA-B-Galactosidase-Based Screening Assay for the Identification of Senotherapeutic Drugs. *J. Vis. Exp.* 58133 (2019) doi:10.3791/58133.

63. Mao, Z., Bozzella, M., Seluanov, A. & Gorbunova, V. DNA repair by nonhomologous end joining and homologous recombination during cell cycle in human cells. *Cell Cycle* **7**, 2902–2906 (2008).

64. Ong, K. T., Mashek, M. T., Davidson, N. O. & Mashek, D. G. Hepatic ATGL mediates PPAR-α signaling and fatty acid channeling through an L-FABP independent mechanism. *J. Lipid Res.* **55**, 808–815 (2014).

65. Gillotin, S., Davies, J. D. & Philpott, A. Subcellular localisation modulates ubiquitylation and degradation of Ascl1. *Sci. Rep.* **8**, 4625 (2018).

66. Rondini, E. A. *et al.* Novel Pharmacological Probes Reveal ABHD5 as a Locus of Lipolysis Control in White and Brown Adipocytes. *J. Pharmacol. Exp. Ther.* **363**, 367–376 (2017).

67. Shang, L. *et al.* Systemic lipolysis promotes physiological fitness in Drosophila melanogaster. *Aging* **14**, 6481–6506 (2022).

68. Renaudin, X. Reactive oxygen species and DNA damage response in cancer. in *International Review of Cell and Molecular Biology* vol. 364 139–161 (Elsevier, 2021).

69. Tubbs, A. & Nussenzweig, A. Endogenous DNA Damage as a Source of Genomic Instability in Cancer. *Cell* **168**, 644–656 (2017).

70. Sathyanarayan, A., Khan, S., Mashek, M. & Mashek, D. ATGL-catalyzed lipolysis regulates SIRT1 to control PGC-1 **a /PPAR- a signaling**. *FASEB J.* **29**, (2015).

71. Abu Shelbayeh, O., Arroum, T., Morris, S. & Busch, K. B. PGC-1α Is a Master Regulator of Mitochondrial Lifecycle and ROS Stress Response. *Antioxidants* **12**, 1075 (2023).

72. Schoors, S. *et al.* Fatty acid carbon is essential for dNTP synthesis in endothelial cells. *Nature* **520**, 192–197 (2015).

73. Ong, A. L. C. & Ramasamy, T. S. Role of Sirtuin1-p53 regulatory axis in aging, cancer and cellular reprogramming. *Ageing Res. Rev.* **43**, 64–80 (2018).

74. Alves-Fernandes, D. K. & Jasiulionis, M. G. The Role of SIRT1 on DNA Damage Response and Epigenetic Alterations in Cancer. *Int. J. Mol. Sci.* **20**, 3153 (2019).

75. McDonnell, E. *et al.* Lipids Reprogram Metabolism to Become a Major Carbon Source for Histone Acetylation. *Cell Rep.* **17**, 1463–1472 (2016).

76. Pougovkina, O. *et al.* Mitochondrial protein acetylation is driven by acetyl-CoA from fatty acid oxidation. *Hum. Mol. Genet.* **23**, 3513–3522 (2014).

77. Di Leo, L. *et al.* Forcing ATGL expression in hepatocarcinoma cells imposes glycolytic rewiring through PPAR-α/p300-mediated acetylation of p53. *Oncogene* **38**, 1860–1875 (2019).

78. Li, S., Shi, B., Liu, X. & An, H.-X. Acetylation and Deacetylation of DNA Repair Proteins in Cancers. *Front. Oncol.* **10**, 573502 (2020).

79. Li, S., Shi, B., Liu, X. & An, H.-X. Acetylation and Deacetylation of DNA Repair Proteins in Cancers. *Front. Oncol.* **10**, 573502 (2020).

80. Ovejero, S. *et al.* A sterol-PI(4)P exchanger modulates the Tel1/ATM axis of the DNA damage response. *EMBO J.* **42**, e112684 (2023).

81. Ting, K. K. Y. *et al.* Intracellular accumulation of free cholesterol in macrophages triggers a PARP1 response to DNA damage and PARP1 impairs lipopolysaccharide-induced inflammatory response. *PLOS ONE* **20**, e0318267 (2025).

82. Markussen, L. K. *et al.* Lipolysis regulates major transcriptional programs in brown adipocytes. *Nat. Commun.* **13**, 3956 (2022).

83. Lord, C. C. *et al.* Regulation of Hepatic Triacylglycerol Metabolism by CGI-58 Does Not Require ATGL Co-activation. *Cell Rep.* **16**, 939–949 (2016).

84. Trayssac, M., Hannun, Y. A. & Obeid, L. M. Role of sphingolipids in senescence: implication in aging and age-related diseases. *J. Clin. Invest.* **128**, 2702–2712 (2018).

85. Seo, K. & Shin, S. M. Induction of Lipin1 by ROS-Dependent SREBP-2 Activation. *Toxicol. Res.* **33**, 219–224 (2017).

86. Sekiya, M., Hiraishi, A., Touyama, M. & Sakamoto, K. Oxidative stress induced lipid accumulation via SREBP1c activation in HepG2 cells. *Biochem. Biophys. Res. Commun.* **375**, 602–607 (2008).

87. Li, A. C. & Glass, C. K. PPAR- and LXR-dependent pathways controlling lipid metabolism and the development of atherosclerosis. *J. Lipid Res.* **45**, 2161–2173 (2004).

88. Chinetti, G., Lestavel, S., Fruchart, J.-C., Clavey, V. & Staels, B. Peroxisome Proliferator-Activated Receptor α Reduces Cholesterol Esterification in Macrophages. *Circ. Res.* **92**, 212–217 (2003).

89. Szántó, M., Gupte, R., Kraus, W. L., Pacher, P. & Bai, P. PARPs in lipid metabolism and related diseases. *Prog. Lipid Res.* **84**, 101117 (2021).

90. Harris, C. A. *et al.* DGAT enzymes are required for triacylglycerol synthesis and lipid droplets in adipocytes. *J. Lipid Res.* **52**, 657–667 (2011).

91. Tyagi, W. & Das, S. Temporal regulation of acetylation status determines PARP1 role in DNA damage response and metabolic homeostasis. *Sci. Adv.* **10**, eado7720 (2024).

92. Smith, A. J. O., Ball, S. S. R., Bowater, R. P. & Wormstone, I. M. PARP-1 inhibition influences the oxidative stress response of the human lens. *Redox Biol.* **8**, 354–362 (2016).

93. Hassa, P. O. *et al.* Acetylation of Poly(ADP-ribose) Polymerase-1 by p300/CREB-binding Protein Regulates Coactivation of NF-κB-dependent Transcription. *J. Biol. Chem.* **280**, 40450–40464 (2005).

94. Tinkum, K. L. *et al.* Fasting protects mice from lethal DNA damage by promoting small intestinal epithelial stem cell survival. *Proc. Natl. Acad. Sci.* **112**, (2015).

95. De La Cruz Bonilla, M. *et al.* Fasting Reduces Intestinal Radiotoxicity, Enabling Dose-Escalated Radiation Therapy for Pancreatic Cancer. *Int. J. Radiat. Oncol.* **105**, 537–547 (2019).

96. Lee, C. *et al.* Fasting Cycles Retard Growth of Tumors and Sensitize a Range of Cancer Cell Types to Chemotherapy. *Sci. Transl. Med.* **4**, (2012).

97. Zaarur, N. *et al.* ATGL-1 mediates the effect of dietary restriction and the insulin/IGF-1 signaling pathway on longevity in C. elegans. *Mol. Metab.* **27**, 75–82 (2019).